The interferon-inducible GTPase MxB promotes capsid disassembly and genome release of herpesviruses

Manutea C Serrero[1,2], Virginie Girault[3], Sebastian Weigang[4], Todd M Greco[5], Ana Ramos-Nascimento[1], Fenja Anderson[1], Antonio Piras[3], Ana Hickford Martinez[1], Jonny Hertzog[6], Anne Binz[1,2,7], Anja Pohlmann[1,2,7], Ute Prank[1], Jan Rehwinkel[6], Rudolf Bauerfeind[8], Ileana M Cristea[5], Andreas Pichlmair[3,9], Georg Kochs[4], Beate Sodeik[1,2,7]*

[1]Institute of Virology, Hannover Medical School, Hannover, Germany; [2]RESIST - Cluster of Excellence, Hannover Medical School, Hannover, Germany; [3]Institute of Virology, Technical University Munich, Munich, Germany; [4]Institute of Virology, Freiburg University Medical Center, University of Freiburg, Freiburg, Germany; [5]Department of Molecular Biology, Princeton University, Princeton, United States; [6]MRC Human Immunology Unit, MRC Weatherall Institute of Molecular Medicine, Radcliffe Department of Medicine, University of Oxford, Oxford, United Kingdom; [7]German Center for Infection Research (DZIF), Hannover-Braunschweig Partner Site, Hannover, Germany; [8]Research Core Unit Laser Microscopy, Hannover Medical School, Hannover, Germany; [9]German Center for Infection Research (DZIF), Munich Partner site, Munich, Germany

*For correspondence:
sodeik.beate@mh-hannover.de

Competing interest: The authors declare that no competing interests exist.

Abstract Host proteins sense viral products and induce defence mechanisms, particularly in immune cells. Using cell-free assays and quantitative mass spectrometry, we determined the interactome of capsid-host protein complexes of herpes simplex virus and identified the large dynamin-like GTPase myxovirus resistance protein B (MxB) as an interferon-inducible protein interacting with capsids. Electron microscopy analyses showed that cytosols containing MxB had the remarkable capability to disassemble the icosahedral capsids of herpes simplex viruses and varicella zoster virus into flat sheets of connected triangular faces. In contrast, capsids remained intact in cytosols with MxB mutants unable to hydrolyse GTP or to dimerize. Our data suggest that MxB senses herpesviral capsids, mediates their disassembly, and thereby restricts the efficiency of nuclear targeting of incoming capsids and/or the assembly of progeny capsids. The resulting premature release of viral genomes from capsids may enhance the activation of DNA sensors, and thereby amplify the innate immune responses.

Editor's evaluation

This paper uses an innovative cell-free protein-protein interaction system to identify factors that interact with HSV-1 capsids in infected cells. In addition to cataloging numerous capsid-interacting proteins, the manuscript probes the antiviral mechanism of one of these, MxB. The data provide strong support for an intriguing model in which MxB "punches" holes in HSV-1 capsids, releasing viral DNA and potentially triggering host DNA sensors. Moreover, the results suggest that viral proteins bind to and shield the capsids from MxB attack, offering a new perspective on how viruses might evade some host defenses.

Introduction

Infections with human alphaherpesviruses are associated with painful and stigmatizing manifestations such as herpes labialis or herpes genitalis, but also cause life-threatening meningitis or encephalitis, potentially blinding eye infections, herpes zoster, and post-herpetic neuralgia, particularly in immunocompromised patients (*Gershon et al., 2015*; *Whitley and Roizman, 2016*; *Whitley and Johnston, 2021*). Herpes simplex viruses (HSV-1, HSV-2) and varicella zoster virus (VZV) productively infect epithelial and fibroblast cells of the skin and mucous membranes as well as neurons, but are restricted in immune cells. Macrophages, Langerhans cells, dendritic cells, and NK cells mount potent immune responses against alphaherpesviruses (*Whitley and Roizman, 2016*).

Intracellular DNA sensors are crucial to sense herpesvirus infections, and to induce caspase-1-mediated inflammation and type I IFN expression (*Hertzog and Rehwinkel, 2020*; *Kurt-Jones et al., 2017*; *Lum and Cristea, 2021*; *Ma et al., 2018*; *Paludan et al., 2019*; *Stempel et al., 2019*). During an unperturbed infection, capsid shells shield herpesviral genomes from cytosolic sensors during nuclear targeting as well as after nuclear genome packaging (*Arvin and Abendroth, 2021*; *Döhner et al., 2021*; *Knipe et al., 2021*). HSV-1 capsids can withstand compressive forces of up to 6 nN which is more than sufficient to endure the 18 atm repulsive pressure of the packaged viral DNA (*Bauer et al., 2013*; *Roos et al., 2009*). So far, it is unclear how cytosolic DNA sensors gain access to herpesviral genomes; either cytosolic host factors disassemble the sturdy herpesviral capsids during infection, or the nuclear envelopes become leaky.

HSV-1 virions contain an amorphous tegument layer that links the icosahedral capsids with a diameter of 125 nm to the viral envelope proteins (*Crump, 2018*; *Dai and Zhou, 2018*; *Diefenbach, 2015*). To identify cytosolic proteins that promote or restrict infection by interacting with HSV-1 capsids, we have developed cell-free methods to reconstitute capsid-host protein complexes using tegumented capsids from extracellular viral particles or tegument-free capsids from the nuclei of infected cells (*Radtke et al., 2014*). Intact capsids are incubated with cytosol prepared from tissues or cultured cells, and the capsid-host protein complexes are isolated, and characterized by mass spectrometry (MS), immunoblot, electron microscopy, and functional assays. We could show that HSV-1 capsids require inner tegument proteins to recruit microtubule motors, to move along microtubules, to dock at nuclear pore complexes (NPCs), to release viral genomes from capsids, and to import viral genomes into the nucleoplasm, and that capsids lacking tegument cannot move along microtubules, but still bind to nuclear pores (*Anderson et al., 2014*; *Ojala et al., 2000*; *Radtke et al., 2010*; *Wolfstein et al., 2006*).

Here, we searched for proteins that might contribute to sensing cytosolic capsids and thereby promote the detection of herpesviral genomes. Using extracts of matured THP-1 cells, a model system for human macrophages (*Tsuchiya et al., 1980*) we identified type I interferon (IFN) inducible proteins that bound specifically to HSV-1 capsids. Among them was the large dynamin-like GTPase myxovirus resistance protein B (MxB). MxB limits the infection of several herpesviruses, and can mediate almost 50% of the IFN-mediated restriction of HSV-1, although its mode of action has remained elusive so far (*Crameri et al., 2018*, *Liu et al., 2012*, *Schilling et al., 2018*, *Jaguva Vasudevan et al., 2018*). MxB has been first described for its potent inhibition of HIV infection (*Goujon et al., 2013*; *Kane et al., 2013*, *Liu et al., 2013*). The human *MX2* gene codes for a full-length MxB (residues 1–715) and a smaller version (residues 26–715) that lacks an N-terminal extension (NTE), which both are highly expressed upon IFN induction (*Melén et al., 1996*). MxB likely operates as an anti-parallel dimer but can also form higher-order filaments; its N-terminal GTPase domain connects to a bundle signaling element that moves relative to the GTPase domain in response to nucleotide binding, and the C-terminal stalk domain is critical for MxB oligomerization (*Alvarez et al., 2017*; *Chen et al., 2017*; *Fribourgh et al., 2014*; *Gao et al., 2011*).

We show here that both, full-length MxB(1-715) and MxB(26-715) have the remarkable property to disassemble the capsids of the three human alphaherpesviruses HSV-1, HSV-2, and VZV, so that they can no longer transport nor shield the viral genomes. Capsid disassembly did not require proteases but depended on the ability of MxB to hydrolyse GTP and to dimerize. As the large tegument protein pUL36 links the capsid vertices to the other tegument proteins (*Crump, 2018*; *Dai and Zhou, 2018*; *Diefenbach, 2015*), and as an increasing amount of associated tegument proteins protected capsids against MxB-mediated disassembly, we propose that MxB attacks the capsids at their vertices. Our data suggest that MxB can bind to and disassemble incoming as well as progeny capsids, and thereby
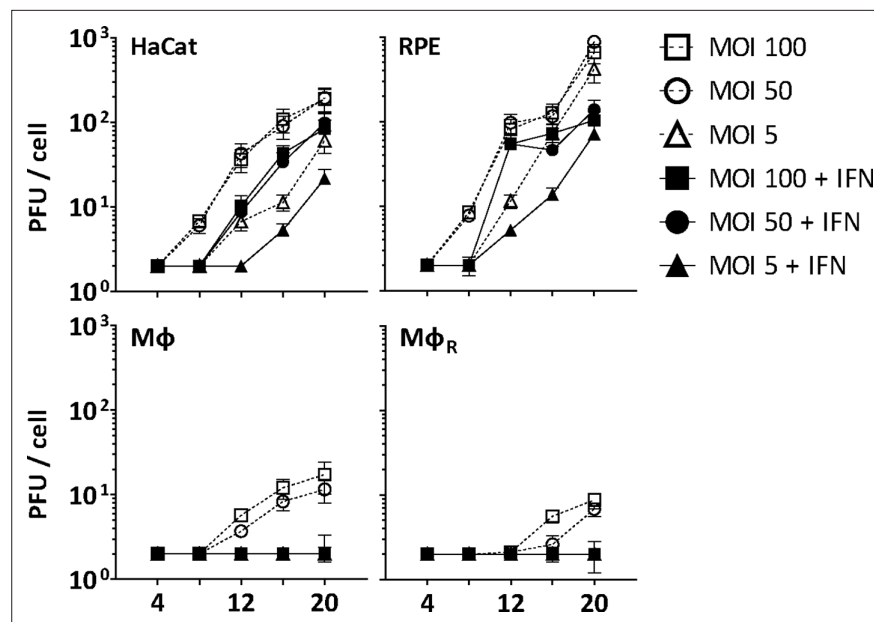
Figure 1. IFN restricts HSV-1 infection in keratinocytes, epithelial cells, and macrophages. HaCat, RPE, Mφ, or Mφ$_R$ cells were mock-treated or treated with human IFN-α (1000 U/mL) for 16 hr and were infected with HSV-1(17$^+$) Lox at 2.5 × 106 (MOI 5), 2.5 × 107 (MOI 50), or 5 × 107 PFU/mL (MOI 100), and the amount of cell-associated and extracellular virions was titrated on Vero cells. Each data point represents the mean of the three technical replicates of the combined cell-associated and extracellular titers. The error bars represent the standard deviation.

might increase the sensing of cytosolic and nuclear viral genomes. Therefore, the MxB GTPase might be the sought-after capsid destroyer that acts upstream of cytosolic or nuclear sensors to promote viral genome detection and induction of innate immune responses.

Results

IFN induction prevents HSV-1 infection of macrophages

Before investigating capsid interactions with macrophage proteins, we compared HSV-1 infection in human keratinocytes (HaCat), pigment epithelial cells (RPE), and THP-1 cells at low, moderate, or high multiplicity of infection (MOI). We stimulated monocyte THP-1 cells with phorbol 12-myristate 13-acetate to differentiate them into a macrophage-like phenotype, and used them either directly (Mφ) or after a resting period of 3 days (Mφ$_R$). HSV-1 replicated productively in HaCat and RPE cells up to 20 hpi, while a pre-treatment with IFN delayed and reduced but did not prevent the production of infectious virions (*Figure 1*). Both Mφ and Mφ$_R$ released 10–100-fold less infectious HSV-1, and an IFN pre-treatment infection at all MOIs. Thus, Mφ and Mφ$_R$ restricted HSV-1 infection efficiently, and the induction of IFN-stimulated genes (ISGs) prevented any productive infection.

IFN-induced protein changes in the cytosol of macrophages

To identify cytosolic macrophage proteins that might foster or restrict HSV-1 capsid functions, we prepared extracts from Mφ$_R$ or IFN-induced Mφ$_{IFN}$ to reconstitute capsid-host protein complexes as they might assemble in macrophages (*Figure 2—figure supplement 1*). Using subcellular fractionation and subsequent dialysis (*Figure 2—figure supplement 2A*), we depleted the extracts of nuclei and mitochondria (*Figure 2—figure supplement 2B*; pellet P1), cytoplasmic membranes such as Golgi apparatus, endoplasmic reticulum and plasma membrane (P1, P2), and small metabolites (S2, S3, S4). Furthermore, most of the cytoskeletal tubulin and actin sedimented into the first pellet (P1), while glyceraldehyde 3-phosphate dehydrogenase (GAPDH), a bona-fide cytosolic protein, remained soluble in the supernatants (S1, S2, S2', S3, S4). Next, we analyzed the proteomes of the Mφ$_R$ and IFN-induced Mφ$_{IFN}$ cytosols at low ATP/GTP concentration [ATP/GTP^{low}] by mass spectrometry (MS; *Supplementary file 1*). We detected 494 (*Figure 2—figure supplement 2C*; black circles)

of more than 600 reported IFN-inducible proteins (***Rusinova et al., 2013***). Of those, a Fisher's exact test identified the interferomeDB, and in particular GALM, COL1A1, LGALS3BP, NT5C3A, IFI44, IFIT2, IFIT3, GBP4, SRP9, IFIT5, DSP, and L3HYPDH as enriched by at least 2.8-fold (log$_2$ 1.5) in the Mφ$_{IFN}$ cytosol (***Figure 2—figure supplement 2C***; red). These changes might reflect IFN-induced transcriptional or translational regulation, post-translational modification, subcellular localization, or susceptibility to proteolysis, and show that the IFN induction had changed the cytosol proteome of the Mφ$_{IFN}$.

HSV-1 capsids interact with specific cytosolic macrophage proteins

To search for cytosolic Mφ proteins whose interactions with HSV-1 capsids depend on their surface composition, we generated tegumented viral V$_{0.1}$, V$_{0.5}$, and V$_1$ capsids as well as D capsids with a reduced tegumentation (***Figure 2—figure supplement 1***). For this, we lysed extracellular particles released from HSV-1 infected cells with non-ionic detergent to solubilize the envelope proteins and lipids, and in the presence of 0.1, 0.5, or 1 M KCl to modify intra-tegument protein-protein interactions (***Anderson et al., 2014***; ***Ojala et al., 2000***; ***Radtke et al., 2010***; ***Radtke et al., 2014***; ***Wolfstein et al., 2006***, ***Zhang and McKnight, 1993***). Furthermore, we dissociated tegument from V$_{0.1}$ capsids by a limited trypsin digestion to generate so-called D capsids. We then incubated similar amounts of different capsid types as calibrated by immunoblot for the major capsid protein VP5 (***Figure 2—figure supplement 2D***) with cytosol at ATP/GTP^{low} from Mφ$_R$ or IFN-induced Mφ$_{IFN}$ for 1 hr at 37 °C. The capsid-host protein complexes assembled in vitro were harvested by sedimentation, and their interactomes were determined by quantitative MS (***Figure 2—figure supplement 1***). As before (***Radtke et al., 2010***; ***Snijder et al., 2017***), the protein intensities were normalized across samples to the abundance of the major capsid protein VP5 (***Supplementary file 2***, host; ***Supplementary file 3***, viral).

Of 2,983 proteins identified (***Supplementary file 2***), we detected 1816 in at least three of the four replicates in any of the eight different capsid-host protein complexes. Of those, 598 host proteins bound differentially to one capsid type over another (***Supplementary file 2***; fold change ≥2 (log$_2$ 1); permutation-based FDR ≤ 0.05). The HSV-1 capsids had recruited specifically 279 proteins of Mφ$_R$ and 390 of Mφ$_{IFN}$ cytosol of which 71 were shared. Hierarchical clustering analyses of the associated Mφ$_R$ or Mφ$_{IFN}$ proteins identified four major classes; for example one enriched on V over D capsids (***Figure 2—figure supplements 3–4***, top green) and one enriched on D over V capsids (***Figure 2—figure supplements 3–4***, bottom violet). Therefore, we further compared the capsid-host interactions of D capsids directly to V$_{0.1}$ (***Figure 2A, D***), V$_{0.5}$ (***Figure 2B and E***), or V$_1$ (***Figure 2C and F***) capsids, and identified 82 proteins of Mφ$_R$ (***Figure 2A, B and C***) and 141 of Mφ$_{IFN}$ (***Figure 2D, E and F***) with 35 being shared (***Supplementary file 2***; difference ≥2.83 fold (log$_2$ 1.5); FDR ≤ 0.01). The Mφ$_R$ capsid-host complexes included 12 and the ones of Mφ$_{IFN}$ 19 proteins listed in the interferome database (***Rusinova et al., 2013***; red in ***Figure 2***). Gene ontology and pathway enrichment analyses showed that the identified 82 Mφ$_R$ (***Figure 3—figure supplement 1***) and 141 Mφ$_{IFN}$ (***Figure 3***) proteins included many proteins implicated in innate immunity, intracellular transport, nucleotide and protein metabolism, as well as intracellular signaling. Overall, the host proteomes of V$_{0.1}$ (red) and D (gray) capsids were rather distinct, but more similar for V$_{0.5}$ (blue) and V$_1$ (green) capsids (***Figure 3—figure supplement 1***, ***Figure 3***). For example, V$_{0.1}$ capsids had recruited specifically the innate immunity proteins PIGR, IGHA1, BPIFA1 and DEFA3, but D capsids LRRFIP1, UFC, C3 and DCD from Mφ$_R$ cytosol. In Mφ$_{IFN}$, the D capsids were enriched for C3, C6, IGBP1, UBA5, UBXN1, UBE3A, and RNF123. These data suggest that protein domains displayed on different capsids interacted with specific cytosolic Mφ$_R$ or Mφ$_{IFN}$ proteins.

In these assays, the capsids interacted with several proteins already validated to promote or restrict HSV or VZV infection. Examples are the ESCRT-III co-factor VPS4 (***Cabrera et al., 2019***; ***Crump et al., 2007***), EIF4H (***Page and Read, 2010***), the Kif2a subunit of kinesin-13 (***Turan et al., 2019***), the POLR1C subunit of RNA polymerase III (***Carter-Timofte et al., 2018***), the DNA protein kinase PRKDC (***Justice et al., 2021***), and DDX1 (***Zhang et al., 2011***). Moreover, the deubiquitinase USP7 (***Rodríguez et al., 2020***) and the ubiquitin ligases RNF123, TRIM72, UFC1 and UBE3A as well as the proteasome might regulate capsid functionality (***Huffmaster et al., 2015***; ***Schneider et al., 2021***) or their degradation (***Horan et al., 2013***; ***Sun et al., 2019***). These data show that HSV-1 capsids exposing a different tegument composition recruited specific cytosolic proteins from resting or IFN-induced macrophages.
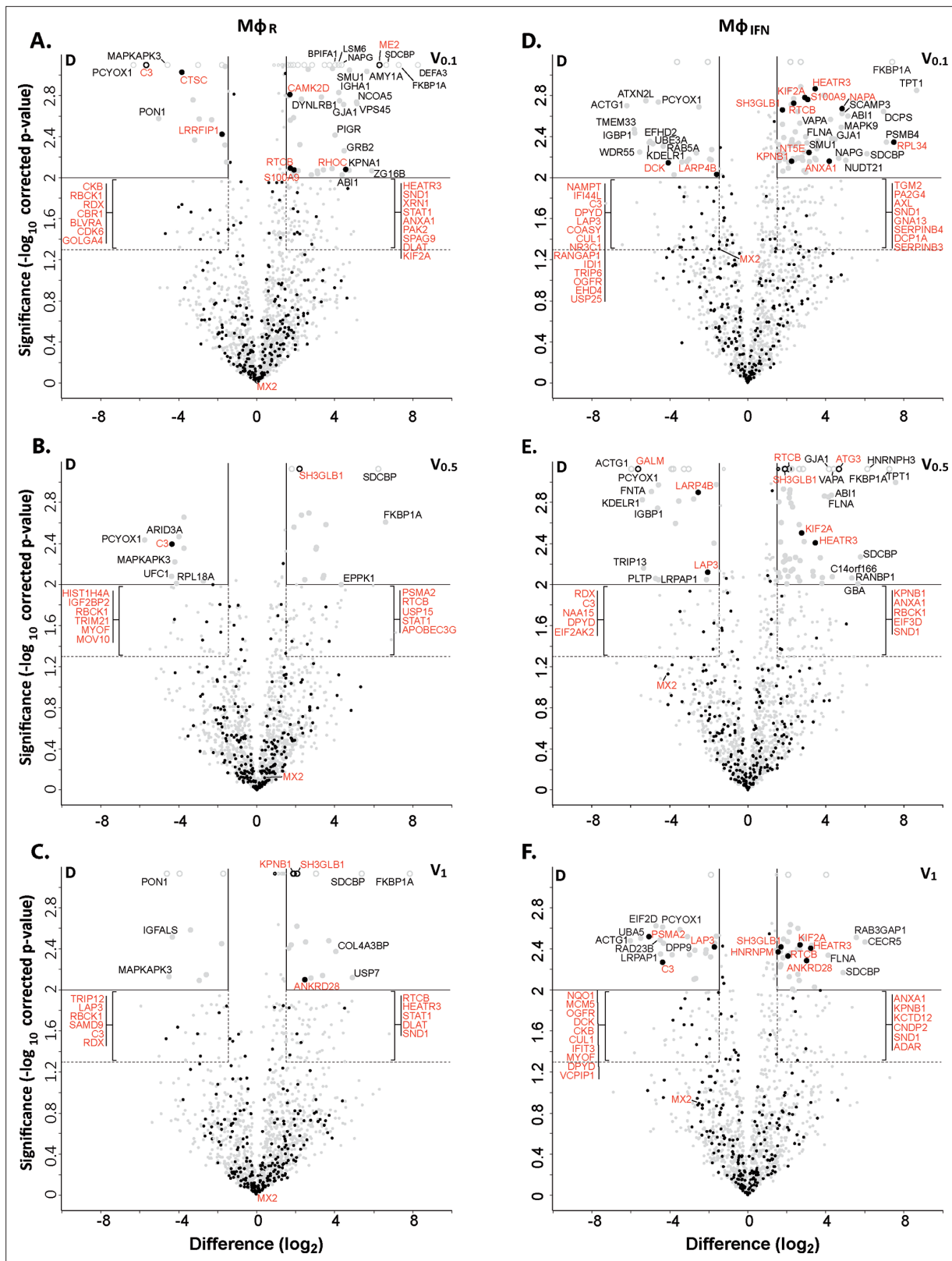
Figure 2. Cytosolic IFN-induced macrophage proteins binding to HSV-1 capsids. Volcano plots of iBAQs counts of proteins identified in capsid-host protein complexes assembled in cytosol from resting THP-1 φ cells (A - C) or treated with interferon-α (D - F) using $V_{0.1}$ (**A, D**), $V_{0.5}$ (**B, E**), or V_1 (**C, F**) capsids in comparison to D capsids. Proteins identified as highly specific interactions are indicated with larger symbols (log$_2$ difference ≥1.5; Welch's t-test, two-tailed, permutation-based FDR ≤ 0.01); those with a log$_2$ difference ≥4 are annotated. ISGs (interferome.org) are indicated by filled black circles,

Figure 2 continued on next page

Figure 2 continued

and are annotated in red if significantly enriched (permutation-based FDR ≤ 0.05, and $\log_2$ difference ≥1.5). Proteins with a q-value = 0 were imputed to $-\log_{10}$ q-value = 3.1 (maximum of the graph), and were indicated with empty circles.

The online version of this article includes the following source data and figure supplement(s) for figure 2:

Figure supplement 1. Experimental strategy to generate host protein-capsid complexes.

Figure supplement 1—source data 1. Characterization of macrophage subcellular fractionation.

Figure supplement 2. Characterization of cytosolic extracts and calibration of capsids.

Figure supplement 3. HSV-1 capsids interactomes.

Figure supplement 4. HSV-1 capsids interactomes.

HSV-1 capsids recruit specific proteins responding to or regulating type I IFN

We next analyzed the Mφ$_{IFN}$ samples in detail as IFN induction had prevented HSV-1 infection completely. We generated cluster maps for the 32 capsid-associated proteins belonging to the GO clusters *Response to type I IFN* or *Regulation of type I IFN production* (*Supplementary file 2*). V capsids recruited DHX9, HSPD1, and FLOT1 as well as proteins involved in the DNA damage response like PRKDC/DNA-PK, XRCC5, and XCCR6 from both, Mφ$_R$ and Mφ$_{IFN}$ cytosol (*Figure 4*). Interestingly, V capsids bound specifically to STAT1 in Mφ$_R$, but to ADAR and IFIT2 in Mφ$_{IFN}$ cytosol. D capsids were enriched for IFI16, OAS2, POLR1C, STAT2, and MxB (gene Mx2) in Mφ$_{IFN}$ but not in Mφ$_R$ (*Figure 4*, *Figure 4—figure supplement 1*). Particularly interesting was the discovery of MxB in these capsid-host protein complexes. MxB was significantly enriched on HSV-1 D capsids in Mφ$_{IFN}$ cytosol, and the IFN treatment had the strongest impact on the interaction of MxB with capsids. Moreover, the calculated enrichment score for MxB on capsids was very high, although the MxB levels in the input cytosol were below the detection limit (undetected, *Figure 2—figure supplement 2*, *Supplementary file 1*). MxB but not its homolog MxA restricts infections of the herpesviruses HSV-1, HSV-2, MCMV, KSHV, and MHV-68, but its mode of action has not been elucidated (*Crameri et al., 2018*, *Liu et al., 2012*, *Schilling et al., 2018*, *Jaguva Vasudevan et al., 2018*). For these reasons, we investigated the interaction of human MxB with HSV-1 capsids further.

MxB binds to capsids

We first characterized the MxB fractionation behavior during the cytosol preparation (*Figure 2— figure supplement 2*). As reported (*Goujon et al., 2013*; *Melén et al., 1996*), MxB was upregulated in IFN-induced Mφ$_{IFN}$. MxB sedimented with nuclei and mitochondria as reported before (*Cao et al., 2020*), and also with cytoplasmic membranes. Moreover, MxB can assemble into cytosolic filaments (*Alvarez et al., 2017*) which might have been sedimented on their own. Both, after the addition of ATP and GTP (ATP/GTP^{high}) or the hydrolase apyrase (*Pilla et al., 1996*; ATP/GTP^{low}), a significant fraction of MxB remained soluble in the cytosol.

Next, we confirmed by immunoblotting that MxB co-sedimented with HSV-1 capsids which had been incubated in cytosols from Mφ$_R$ or Mφ$_{IFN}$. In line with the MS results, MxB bound better to D than to V$_{0.1}$, V$_{0.5}$, or V$_1$ capsids (*Figure 5A*). We next probed authentic nuclear capsids, namely empty A, scaffold-filled B, or DNA-filled C capsids, as well as tegumented V$_1$, V$_{0.5}$, V$_{0.1}$ or D capsids with cytosol of A549-MxB(1-715) epithelial cells expressing MxB(1-715). Nuclear A and C as well as V$_1$ and D capsids recruited MxB efficiently, while B, V$_{0.1}$ and V$_{0.5}$ capsids bound less MxB (*Figure 5B*). MxB did not sediment by itself, and also did not associate with agarose beads used as another sedimentation control (*Figure 5A and B*). These data indicate that MxB binds to specific structural features on the capsid surface.

In cells, MxB-mediated restriction of herpesvirus replication depends on its N-terminal 25 amino acid residues (NTE), its GTPase activity, and its capacity to form dimers (*Crameri et al., 2018*; *Schilling et al., 2018*; *Jaguva Vasudevan et al., 2018*). We incubated capsids with cytosols containing MxA, MxB(1-715), MxB(26-715) (*Melén et al., 1996*; *Melén and Julkunen, 1997*), MxB(K131A) with reduced GTP binding, MxB(T151A) lacking the GTPase activity, or MxB(M574D) unable to dimerize (*Alvarez et al., 2017*; *Fribourgh et al., 2014*; *King et al., 2004*; *Schilling et al., 2018*). In contrast to MxA, MxB(1-175), MxB(26-715), and MxB(M574D) co-sedimented with capsids to a similar extent.
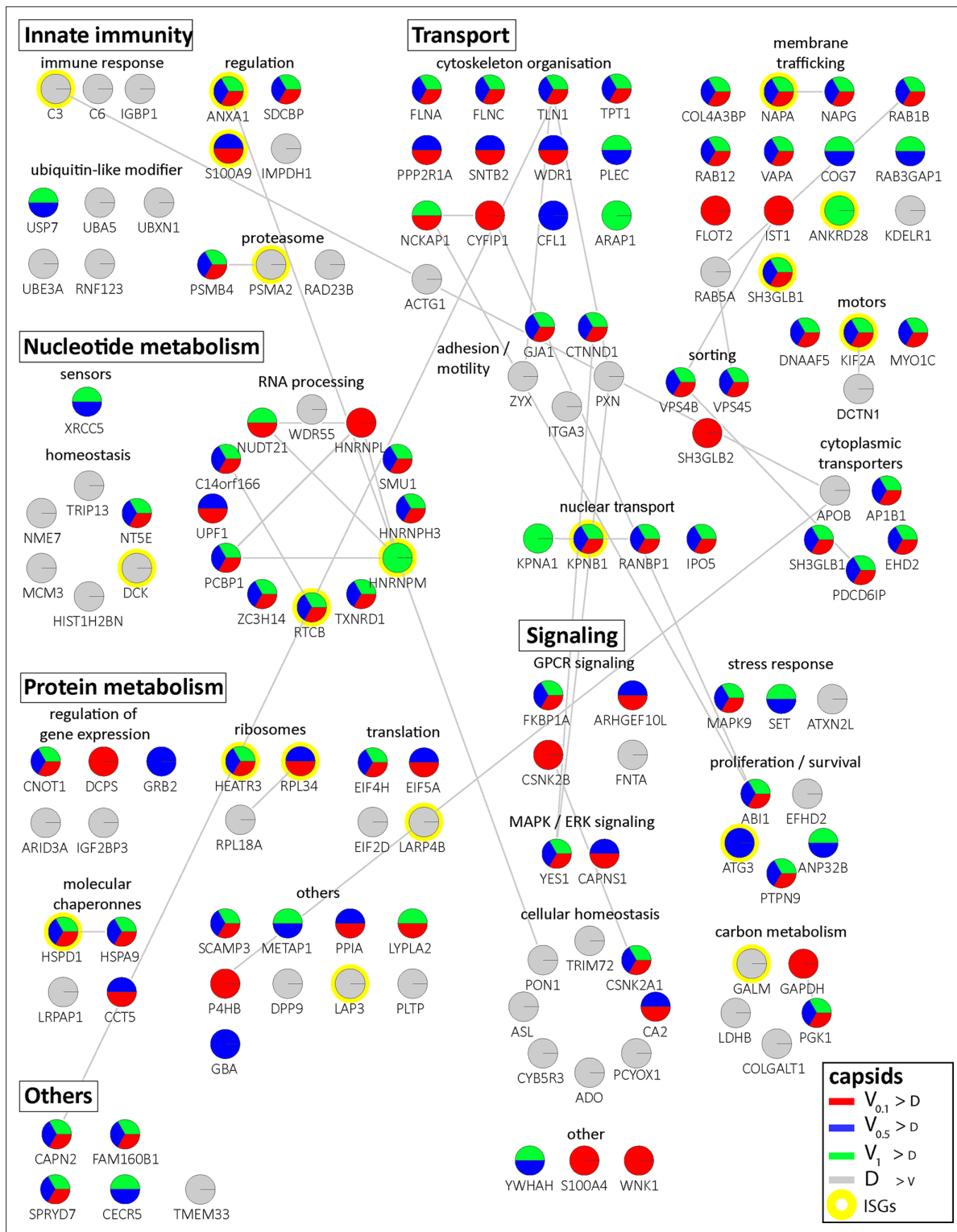
Figure 3. Cytosolic proteins of IFN-induced macrophages binding to HSV-1 capsids. Host proteins from cytosol of IFN-stimulated Mφ$_{IFN}$ (c.f. D, E, F; abundance log$_2$ difference larger than 1.5; significance permutation-based FDR smaller than 0.01) interacting with V$_{0.1}$, V$_{0.5}$, V$_1$, or D capsids were assembled into a functional interaction network of known protein-protein-interactions (gray lines; STRING database, confidence score of 0.7), and grouped according to their known functions (Gene Ontology, Pathway analysis). The Pie chart for each protein indicates its relative enrichment on V$_{0.1}$ (red), V$_{0.5}$ (blue), V$_1$ (green), or D capsids (gray).

The online version of this article includes the following figure supplement(s) for figure 3:

Figure supplement 1. Cytosolic proteins of resting macrophage binding to HSV-1 capsids.
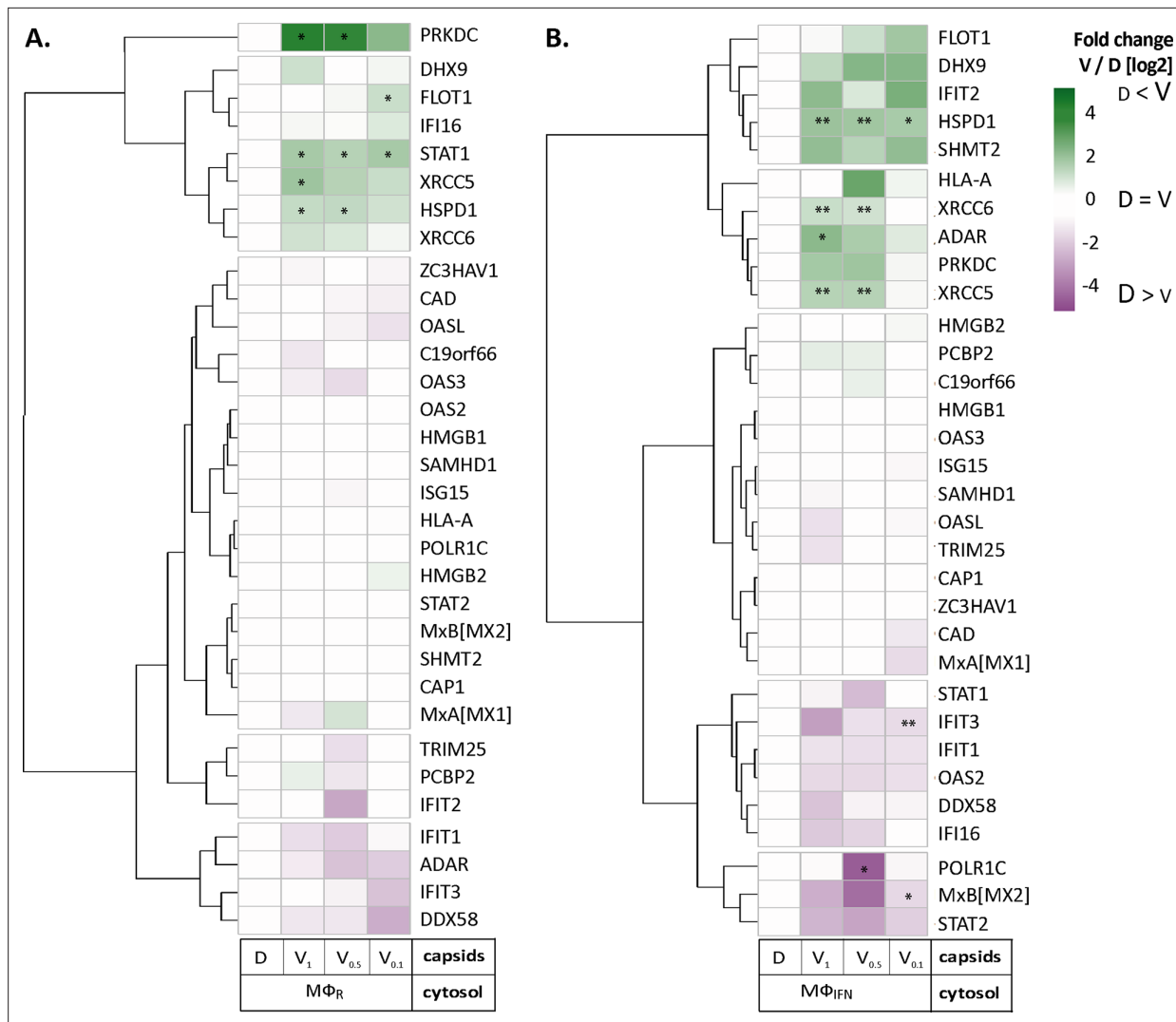
Figure 4. HSV-1 capsids associate with proteins involved in type I IFN response. Unbiased hierarchical clustered heat map showing the $\log_2$ fold changes of IFN-induced proteins (GO type-I IFN) identified from capsids-host protein sediments from cytosol of resting Mφ, or IFN-induced Mφ$_{IFN}$ macrophages. For each protein, the fold change was calculated based on their abundance (iBAQs) in V_1, $V_{0.5}$, and $V_{0.1}$ capsids as compared to their abundance in D capsids, using a linear scale from violet being the lowest to dark green being the highest. (*) and (**) design the proteins with an FDR corrected p-value ≤ 0.05 and ≤ 0.01, respectively.

The online version of this article includes the following figure supplement(s) for figure 4:

Figure supplement 1. HSV-1 capsids binds to a few ISG proteins.

Interestingly, MxB(K131A) did not bind to capsids, while MxB(T151A) bound even stronger (*Figure 5C*). These data suggest that conformational changes associated with GTP binding or hydrolysis contribute to MxB interaction with HSV-1 capsids.

MxB disassembles capsids of alphaherpesviruses

Next, we tested whether MxB might affect HSV-1 capsid stability. While the previous capsid sedimentation assays were performed at ATP/GTP^{low}, they suggested that the GTP/GDP state of MxB might modulate its interaction with capsids. To test this experimentally, we supplemented the cytosols with 1 mM GTP, 1 mM ATP, and 7.5 mM creatine phosphate to maintain high ATP/GTP levels [ATP/GTP^{high}]. We resuspended sedimented capsid-host protein complexes and applied them onto EM grids (*Figure 2—figure supplement 1*), or we added isolated capsids directly onto EM grids and then placed them on a drop of cytosol to allow the formation of capsid-host protein complexes (*Figure 6A*). This direct *on-grid assay* required 50 times fewer capsids than the *sedimentation-resuspension assay*
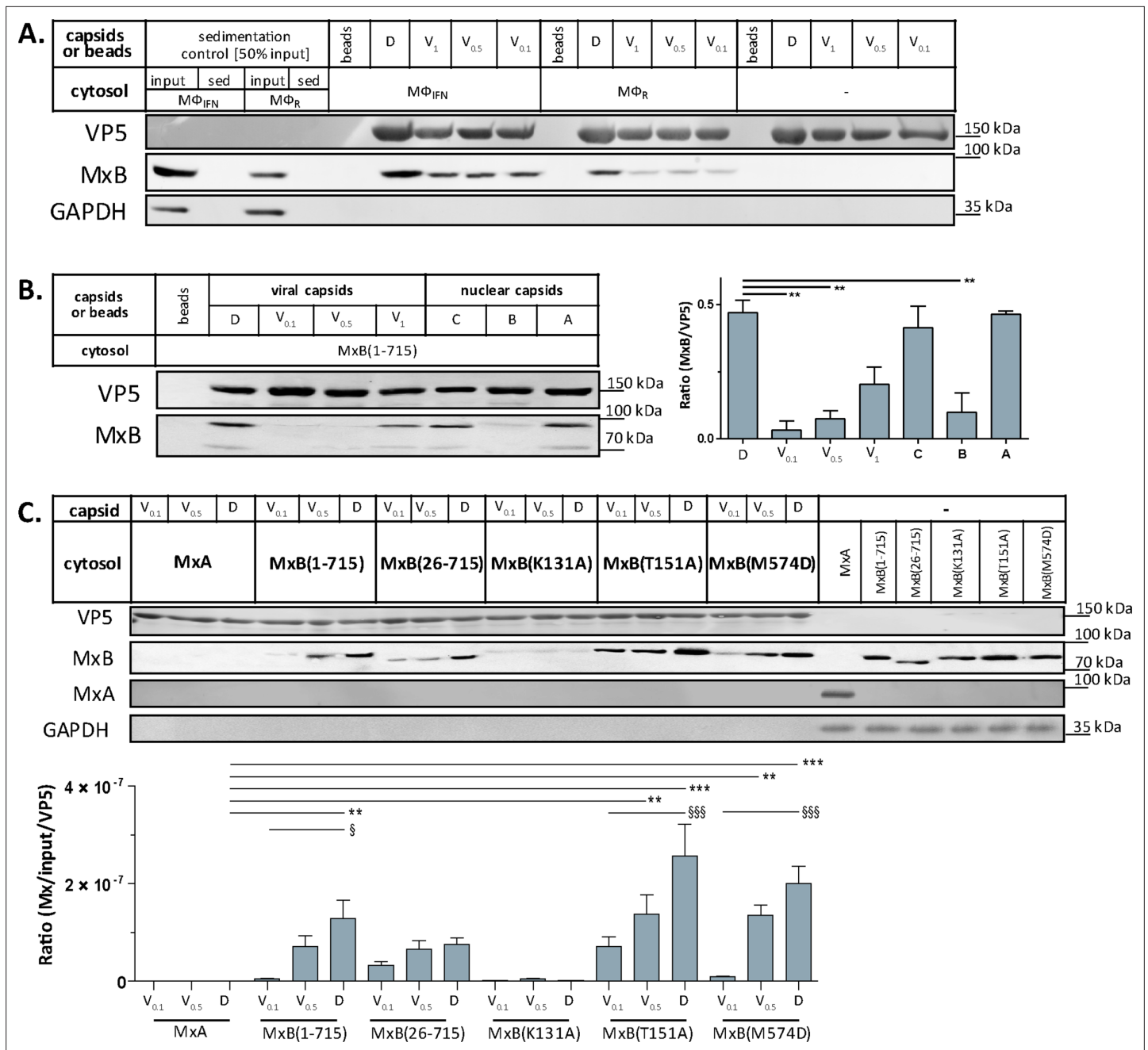
Figure 5. Tegumentation reduces MxB binding to HSV-1 capsids. The binding of MxB to viral $V_{0.1}$, $V_{0.5}$, V_1, or D, or to nuclear A, B, or C capsids was analyzed after incubation in 0.2 mg/mL cytosol prepared from (A; *Figure 5—source data 1*) THP-1 φ stimulated or not with IFN, or (B-C; *Figure 5—source data 1*; *Figure 5—source data 1*) A549 cells stably expressing MxA, MxB(1-715) full length, the short MxB(26-715), or MxB mutants defective in GTP-hydrolysis MxB(T151A), GTP-binding and hydrolysis MxB(K131A), or dimerization MxB(M574D). Sedimented capsid-host protein complexes were then analyzed by immunoblot for VP5 (capsid), MxB, MxA, and GAPDH as a loading control. As control cytosols were sedimented without capsids (A: sed), or with uncoated agarose beads (A, B: beads). The amounts of MxA/MxB found in the capsid-host protein complexes were quantified, and normalized to their respective VP5 levels. Error bars: SEM. summarized from three experiments. One asterisk denotes $p < 0.05$, two asterisks indicate $p < 0.01$ and three asterisks represent $p < 0.001$ as determined by Welch's t-tests comparisons.

The online version of this article includes the following source data for figure 5:

Source data 1. Cytosolic MxB from THP-1 cells co-sediments with capsids in *Figure 5A*.
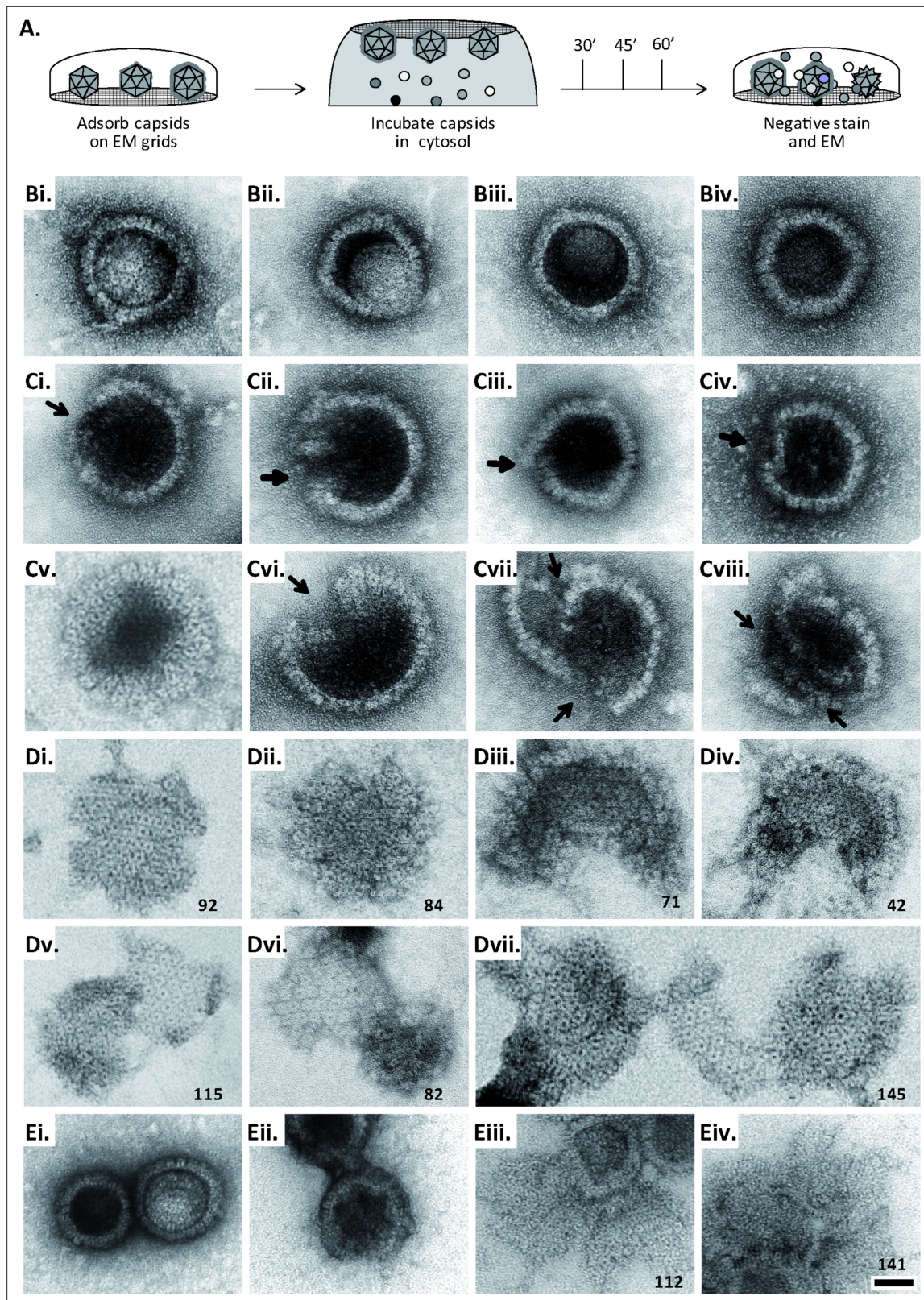
Figure 6. MxB induces disassembly of herpesviral capsids. (**A**) Experimental design: Capsids were adsorbed onto hydrophilic enhanced carbon-coated EM grids for 20 min at RT. The capsids were incubated in cytosol with ATP/GTP^{high}, and the incubation was stopped at different times by extensive washing. The samples were analyzed by EM after negative staining with uranyl acetate. (**B–D**) Capsids after incubation in cytosol derived from rested Mφ or IFN-induced Mφ$_{IFN}$ macrophages, or control or MxB(1-715) A549 expressing cells for 1 hr at 37 °C, and classified as (**B**) intact, (**C**) punched or

Figure 6 continued on next page

Figure 6 continued

(**D**) disassembled flat phenotypes. The number of capsomers per flat particle was counted, and is displayed at the bottom of each figures. (**E**) Nuclear VZV capsids remain intact (Ei) after incubation in the cytosol of A549 control cells, or but appear punched (Eii) or as flat shells (Eiii, Eiv) after incubation in the cytosol of A549 cells expressing MxB. Scale bar: 50 nm.

The online version of this article includes the following figure supplement(s) for figure 6:

Figure supplement 1. Capsid disassembly intermediates by anti-capsid immunoEM.

and allowed for time-course analyses. For both, we negatively contrasted the samples with uranyl acetate and analyzed them by electron microscopy.

When capsids were incubated with cytosol from A549 control cells not containing MxB, we saw mostly intact capsids with an appropriate diameter of about 125 nm, and an intact icosahedral morphology characterized by pentons at the vertices and hexons on the triangular capsid faces (*Figure 6B*). The capsids contained genomic DNA as the uranyl acetate used for negative contrast staining had not or only partially entered the capsid lumen. But a treatment with cytosol from IFN-induced Mφ$_{IFN}$ or A549-MxB(1-715) cells dramatically impaired the capsid shell. Based on different MxB-induced morphological changes, we classified the capsid structures that we had identified by immunolabeling for capsid proteins (*Figure 6—figure supplement 1*) into three categories. *Intact capsids* (*Figure 6B*, Figure S6A) have an icosahedral morphology and include empty A, scaffold-filled B, and DNA-filled C capsids. *Punched capsids* are characterized by indentations on one or more vertices and an impaired icosahedral shape (*Figure 6C*, *Figure 6—figure supplement 1B*). *Flat shells* have completely lost their icosahedral shape (*Figure 6D*, *Figure 6—figure supplement 1C*). We estimated the number of capsomers on *flat shells* based on their area, and scored a structure with <100 capsomers as a half capsid and with ≥100 as one capsid (numbers in *Figure 6D*). Cytosols containing MxB(1-715) also disassembled capsids of HSV-2 (not shown) or VZV (*Figure 6E*) to *punched capsids* and *flat shells*. As MxB induced capsid disassembly of HSV-1, HSV-2, and VZV, these experiments suggest that MxB restricts the infection of herpesviruses by targeting their capsids.

MxB requires GTP hydrolysis and dimerization to attack herpesviral capsids

Next, we further characterized the capsid disassembly activity of MxB by quantitative electron microscopy. Cytosol from IFN-induced Mφ$_{IFN}$ disassembled more than 80% of the capsids within 1 hr while resting Mφ$_R$ disassembled only about 40% (*Figure 7A*). Cytosol derived from A549 control cells had a minor effect on capsids, while cytosol from A549-MxB(1-715) cells disassembled capsids almost as efficiently as cytosol from Mφ$_{IFN}$. Spiking cytosol from A549 control cells with an increasing percentage of A549-MxB(1-715) cytosol led to an increasing capsid disassembly with a majority of *punched capsids*, at 50% or 66% MxB cytosol, while incubation in pure A549-MxB(1-715) cytosol lead to more than 95% disassembly to mostly *flat shells* within 1 hr of incubation (*Figure 7B*). We then asked whether MxB had activated other host proteins to mediate capsid disassembly, or whether it was directly responsible. We prepared cytosol from A549-MxB(1-715)-MxB(26-715) expressing both untagged MxB proteins, or from A549-MxB-FLAG expressing both MxB(1-715)-FLAG and MxB(26-715)-FLAG. Both cytosols promoted capsid disassembly (MxB; MxB-FLAG in *Figure 7C*). An immunodepletion with anti-FLAG antibodies removed only the FLAG-tagged MxB proteins (*Figure 7—figure supplement 1*), and accordingly the disassembly activity from the A549-MxB-FLAG cytosol (MxB-FLAG FT), but not from the A549-MxB(1-715)-MxB(26-715) cytosol (MxB FT) containing both untagged MxB proteins.

We next tested at ATP/GTP^{high} the effect of various MxB mutants on HSV-1 capsid stability. While full-length MxB(1-715) induced capsid disassembly, the MxB mutants impaired in GTPase activity (T151A), GTP binding (K131A), or dimerization (M574D) as well as cytosol with MxB at ATP/GTP^{low} did not (*Figure 7D*). In contrast, the smaller MxB(26-715) protein lacking the NTE retained about 50% of the capsid disassembly activity. Furthermore, studying the stability of capsids pre-adsorbed *on-grid* in a time-course revealed a lag phase of about 30 min until broken capsids appeared with increasing rate (*Figure 7E*). The percentage of *punched capsids* reached a plateau at 50 min, while the amount of *flat shells* continued to increase (*Figure 7E*). Further experiments showed that MxB attacked D capsids more efficiently than tegumented V$_{0.5}$ capsids, of which about 70% resisted the MxB attack (*Figure 7F*). In contrast, the V$_{0.1}$ capsids seemed to be spared from MxB attack, since no
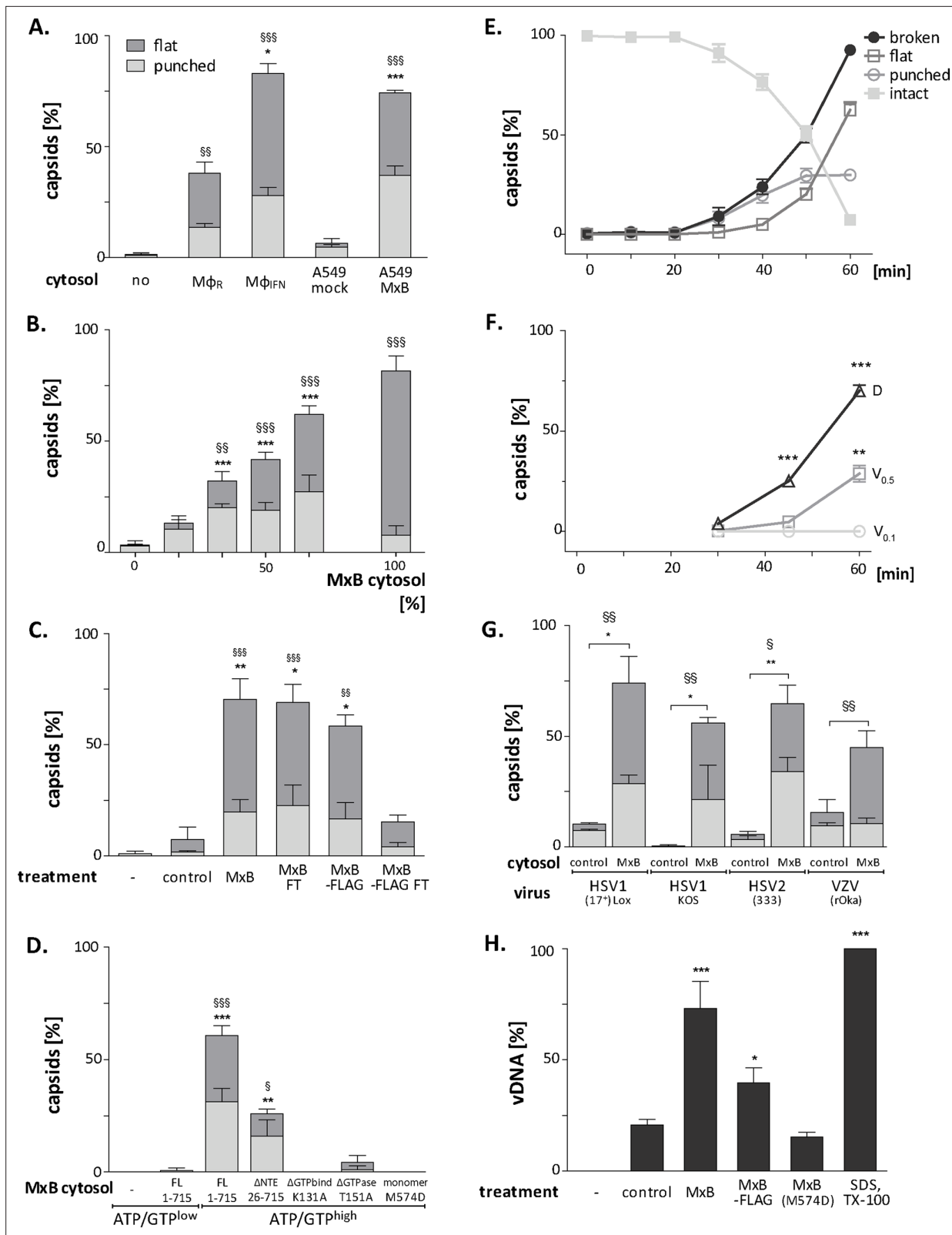
Figure 7. MxB GTP hydrolysis and dimerization required for capsid disassembly and vDNA release of viral genomes. HSV-1 (**A–H**), HSV-2 (**G**) or VZV capsids (**G**) were incubated with cytosol at ATP/GTP^high for 1 hr or the indicated time (**E,F**) at 37 °C, and classified into *intact*, *punched* and *flat* capsids by electron microscopy (**A–G**), or the amount of released viral DNA was measured by qPCR (**H**). (**A**) Quantification of *punched* and *flat* D capsid shells in cytosol prepared from rested Mφ or IFN-induced MφIFN macrophages, or from control A549 (mock) or A549-MxB(1-715) cells. (**B**) Increasing amounts

Figure 7 continued on next page

Figure 7 continued

of MxB(1-715) [%] were added to control A549 cytosol, and the amounts of *punched* and *flat* capsids were quantified after incubation in these mixtures. (**C**) Cytosols of A549 cells expressing MxB(1-715) and Mx(25-715) or MxB(1-715)-FLAG and MxB(26-715)-FLAG were incubated with anti-FLAG antibodies coupled to magnetic beads, the flow-through fractions (FT) were harvested, capsids were treated with anti-FLAG treated or control cytosols, and the amount of punched and flat capsids were quantified. (**D**) Capsids were incubated in cytosols prepared from A549 cells expressing full-length (FL) MxB(1-715), MxB(26-715), MxB(K131A), MxB(T151A), or MxB(M574D) at ATP/GTP^{low} or ATP/GTP^{high} levels. (**E**) Time-course of MxB-induced disassembly of capsids pre-adsorbed onto EM grids, incubated with cytosol from A549-MxB(1-715). (**F**) Analysis of D, V$_{0.5}$, or V$_{0.1}$ capsids treated with MxB(1-175) cytosol for *broken* (*punched* +*flat*) capsids after negative stain and EM as described for panel E. (**G**) Quantification of MxB cytosol disassembly of D capsids of HSV-1(17$^+$)Lox, HSV-1(KOS), or HSV-2(333), or nuclear C capsids of VZV, after incubation in cytosol from A549-MxB(1-715) cells. (**H**) D capsids were incubated with different cytosols for 1 hr at 37 °C or treated with 1% SDS and 10% Tx-100 only, and the released DNA not protected by capsid shells was quantified by qPCR. Error bars: SEM from 100 capsids in three biological replicates. One symbol of *or § denotes p < 0.05, two p < 0.01, and three p < 0.001 as determined in One-way analysis of variance with a Bonferroni post-test, and comparing the relative amounts of (*) *punched* and (§) *flat* capsids, or indicating the differences with the mock-treated samples (*).

The online version of this article includes the following source data and figure supplement(s) for figure 7:

Figure supplement 1. Cytosol immunodepleted for MxB.

Figure supplement 1—source data 1. Western blot of MxB immunodepletion.

broken capsids appeared within an 1 hr treatment. Since MxB restricts infection of several herpesviruses (*Crameri et al., 2018*, *Liu et al., 2012*, *Schilling et al., 2018*, *Jaguva Vasudevan et al., 2018*), we compared the impact of MxB on D capsids from HSV-1(17$^+$)Lox, HSV-1(KOS), HSV-2(333), or on nuclear C capsids from VZV(rOka). Capsids of these human alphaherpesviruses were all susceptible to MxB attack (*Figure 7G*).

MxB attack leads to the release of viral genomes from capsids

Next, we determined how well the capsid shells protected the viral genomes against a DNA nuclease digestion. Capsids released three or two times more viral genomes in cytosols from MxB(1-715) or MxB-FLAG than from control or MxB(M574D) cells (*Figure 7H*). Together, these data indicate that the MxB GTPase disassembles the capsid shells and induces a release of viral DNA of several herpesviruses. Our experiments suggest that GTP binding and hydrolysis as well as dimerization contribute to MxB-mediated disassembly of alphaherpesvirus capsids. Its slow start with a lag of about 30 min indicates that the capsid attack might require some nucleating or cooperative reaction to assemble active MxB oligomers or an MxB-containing complex onto capsids.

Tegument proteins protect against MxB attack

As complete tegumentation shielded V$_{0.1}$ capsids against destruction, while MxB bound to surface features exposed on V$_{0.5}$, A, C and D capsids, we compared the proteomes of the V$_{0.1}$, V$_{0.5}$, V$_1$, and D capsids. We calibrated the relative abundances of the 58 HSV-1 proteins detected to the normalized amounts of the major capsid protein VP5. The tegument compositions of V$_{0.1}$, V$_{0.5}$, and V$_1$ capsids were similar to each other but different from D capsids (*Figure 8*). The bona-fide capsid proteins VP21, VP24, VP22a, VP19c, and VP23 varied little among all capsid types. However, D capsids contain a bit less capsid surface proteins; namely VP26, the capsid specific vertex components (CSVC) pUL17 and pUL25, and to some extent the portal pUL6, and less of the major tegument proteins VP22, VP13/14, VP16, VP11/12 as well as other tegument proteins with ICP0, pUL36, and pUL37 being most susceptible to the trypsin treatment. Overall, there were little differences in the relative tegument protein amounts among V$_{0.5}$ and V$_1$ capsids. In contrast, V$_{0.1}$ capsids contained more tegument proteins, for example VP13/14, pUS3, and pUL16. All capsid preparations contained traces of membrane proteins and nuclear HSV-1 proteins contributing to DNA replication and packaging (*Figure 8—figure supplement 1*). These data further validated that a treatment with 0.5 or 1 M KCl during the detergent lysis of virions destabilized intra-tegument interactions. Furthermore, the limited trypsin digestion had reduced the capsid proteome further and increased the susceptibility to MxB attack.

Discussion

Cell-type-specific defence mechanisms shape the arms race between proteins restricting or promoting nuclear targeting of incoming viral capsids and viral genome release into the nucleoplasm. We have
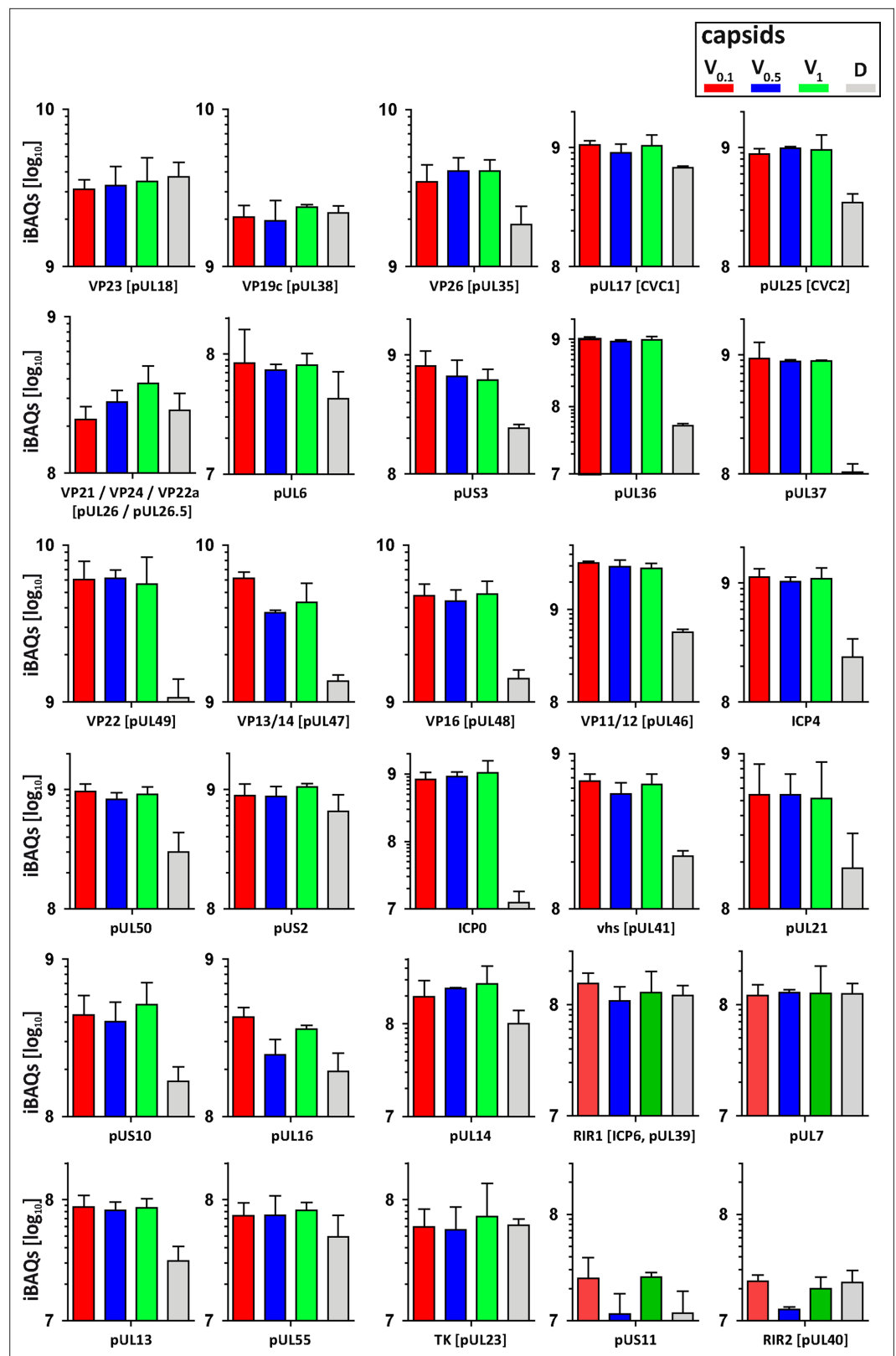
Figure 8. Structural and tegument characterization of $V_{0.1}$, $V_{0.5}$, V_1, and D capsids. The composition of HSV-1(17+) Lox derived $V_{0.1}$ (red), $V_{0.5}$ (blue), V_1 (green), and D (gray) capsids was analyzed by quantitative mass spectrometry in four biological replica. The sum of all the peptides intensities (iBAQ, intensity-based absolute quantification)

Figure 8 continued on next page

Figure 8 continued

of each viral protein known to participate in the structure of the capsids was normalized to the one of VP5 and displayed in a bar plot for each viral protein.

The online version of this article includes the following figure supplement(s) for figure 8:

Figure supplement 1. Membrane and non-structural proteins on V capsids versus D capsids.

developed biochemical assays to investigate functional interactions of viral capsids with host cell structures (*Radtke et al., 2014*), and analyzed here HSV-1 capsid-host protein complexes assembled in cytosols from resting $M\varphi_R$ or IFN-induced $M\varphi_{IFN}$ cells. We show that the IFN-inducible MxB GTPase bound to alphaherpesviral capsids, most likely to structural features around the capsid vertices, and disassembled herpesvirus capsids in a GTP-dependent fashion, and so that they no longer shielded the viral genomes. Capsid disassembly by MxB could reduce nuclear targeting of incoming capsids and genomes, but stimulate the activation of cytosolic DNA sensors and innate immune responses.

Cytosolic IFN-induced macrophage proteins binding to HSV-1 capsids

IFN induction prevented HSV-1 infection of $M\varphi$, and increased the cytosolic abundance of at least 12 proteins listed in the interferome database (*Rusinova et al., 2013*). Here, we assembled host protein-capsid complexes from HSV-1 capsids and cytosols of $M\varphi$ or $M\varphi_{IFN}$ cells as they might also form in cells. While our MS analyses showed that $V_{0.5}$ and V_1 capsids recruited unique but also common proteins, the proteomes of $V_{0.1}$ and D capsids were more distinct. These specific interactions are consistent with the notion that a treatment with 0.5 or 1 M KCl during the detergent lysis of virions destabilized intra-tegument interactions, that influenced, for example, the recruitment of dynactin, kinesin-1, and kinesin-2 from brain cytosol (*Ojala et al., 2000*; *Radtke et al., 2010*; *Wolfstein et al., 2006*). Moreover, these results are consistent with immunoelectron microscopy data showing that the surface of distinct V capsid types display different tegument epitopes (*Radtke et al., 2010*), and with cryoelectron tomography data revealing diminishing tegument densities from $V_{0.1}$, $V_{0.5}$, V_1, capsids to C capsids (*Anderson et al., 2014*). Thus, the surface features of $V_{0.1}$, $V_{0.5}$, and V_1 capsids differ as indicated by cryoelectron tomography, binding of anti-tegument antibodies, and the recruitment of distinct sets of cytosolic proteins from brain tissue (*Radtke et al., 2010*), or macrophages as shown here. Host proteins may bind to viral proteins in both states, when they are soluble in the cytosol or the nucleoplasm, or when they are associated with capsids. From host proteins shown here to bind to capsids, direct interactions with tegument proteins have already been reported; for example USP7 binding to ICP0 (*Everett et al., 1997*) or EIF4H binding to vhs (pUL41; *Page and Read, 2010*). Furthermore, proteins involved in intracellular trafficking or virus assembly associated particularly with tegumented V capsids. For example, importin α5 (*KPNA1*) might mediate capsid targeting to the nuclear pores (*Döhner et al., 2018*; *Döhner et al., 2021*), while RAB1B contributes to the envelopment of cytosolic HSV-1 capsids (*Zenner et al., 2011*).

MxB binding to alphaherpesviral capsids

In addition to MxB, the host-capsid complexes included other antiviral proteins which in turn might be counteracted by HSV-1 proteins. Several $M\varphi_{IFN}$ proteins already know to restrict herpesviruses, for example STAT2, POLR1C, IFI16, DDX58 (RIG-I), and OAS2 (*Kurt-Jones et al., 2017*; *Lum and Cristea, 2021*; *Ma et al., 2018*), bound preferentially to D capsids. As it was not known how MxB might restrict herpesviral infection (*Crameri et al., 2018*; *Schilling et al., 2018*; *Jaguva Vasudevan et al., 2018*), we investigated its association with capsids further. B capsids are less sturdy and have not undergone the structural changes that stabilize the A and C capsids (*Roos et al., 2009*; *Sae-Ueng et al., 2014*; *Snijder et al., 2017*). Intriguingly, this stabilization depends on the CSVC proteins pUL17 and pUL25 (*Sae-Ueng et al., 2014*; *Snijder et al., 2017*), which are present on B, A, and C capsids (*Anderson et al., 2014*; *Radtke et al., 2010*; *Snijder et al., 2017*). As MxB bound to A, C and D, but not to B capsids, it might recognize surface features formed during capsid stabilization, e.g. matured CSVCs or portals, which are increasingly shielded on tegumented V_1, $V_{0.5}$, and $V_{0.1}$ capsids.

MxA and MxB GTPases inhibit several viruses by blocking early steps of infection (*Haller et al., 2015*). MxB binding to HIV capsids depends on its N-terminal region (NTR) of about 90 residues and the GTPase domain (*Betancor et al., 2019*; *Fricke et al., 2014*; *Smaga et al., 2019*; *Xie et al., 2021*).

Similarly, HSV-1 capsids bound MxB(1-715) and to a lesser extent MxB(26-715). But in contrast to HIV capsids (*Betancor et al., 2019*; *Xie et al., 2021*), HSV-1 capsids recruited also the GTPase deficient MxB(T151A) and the monomeric MxB(M574D). These data indicate that the interaction of MxB with HSV-1 capsids depends on the NTE of 25 residues, its GTP/GDP status, but not on its dimerization.

MxB induced disassembly of alphaherpesviral capsids

HSV-1 capsid disassembly did not require proteolysis as the cytosols contained protease inhibitors, but may be modulated by other host proteins as there was a considerable lag phase. MxB did not attack fully tegumented $V_{0.1}$ capsids, while $V_{0.5}$ or D capsids were more susceptible. The large tegument protein pUL36 links other tegument proteins to the capsids; it is tightly associated with pUL17 and pUL25 at the CSVCs at the pentons, and it extends toward the twofold symmetry axes connecting neighboring capsid faces (*Coller et al., 2007*, *Liu et al., 2017*, *Newcomb and Brown, 1991*, *Roos et al., 2009*, *Schipke et al., 2012*). Our electron microscopy data suggest that MxB attacked the fivefold symmetry axes as the *punched capsids* had dramatic dents on the capsid vertices. MxB might furthermore attack the portal cap, a cap of HSV1-pUL25 or its homologs in other herpesviruses, which seals the pUL6 portal after DNA packaging is completed (*Liu et al., 2019*, *McElwee et al., 2018*; *Naniima et al., 2021*). The high internal capsid pressure due to the negatively charged genome (*Bauer et al., 2013*; *Roos et al., 2009*) could support the MxB attack from the outside. The limited trypsin treatment might have primed the D capsids for disassembly, as they contained less pUL36, pUL17, pUL25, and pUL6 than the V capsids. However, MxB also attacked $V_{0.5}$ capsids that resemble cytosolic capsids during nuclear targeting or after nuclear egress (*Ojala et al., 2000*; *Wolfstein et al., 2006*; *Radtke et al., 2010*; *Anderson et al., 2014*); just not as fast, and not as efficient. Altogether, these results suggest that increasing tegumentation protects incoming and newly assembled capsids, possibly by masking the MxB target structure, or by inhibiting its GTPase cycle.

The MxB-mediated capsid disassembly required its NTE(1-25), GTP hydrolysis, and dimerization. For the homologous MxA GTPase that limits infection of many RNA viruses (*Haller et al., 2015*), *Gao et al., 2011* proposed a restriction mechanism that involves GTP hydrolysis and a mechano-chemical coupling within ring-like oligomers with the GTPase domains being exposed on their outer diameter (*Gao et al., 2011*). Similarly, MxB can also assemble into helical tubes with the NTE and the GTPase domain oriented outwards (*Alvarez et al., 2017*). Accordingly, MxB monomers and dimers might associate with the capsid vertices and insert between the hexons of neighboring capsid faces. A further oligomerization of MxB and/or conformational changes associated with GTP hydrolysis might then exert destabilizing forces onto the capsid shells, and ultimately push the capsid faces apart.

Does MxB induce capsid disassembly in cells?

Future studies need to investigate whether MxB also induces the disassembly of herpesviral capsids in cells. Upon docking of an incoming capsid to a NPC, the pUL25 portal cap is supposed to be displaced, the pUL6 portal to be opened, and the DNA to be ejected from the capsid into the nucleoplasm due to this intramolecular repulsion (*Brandariz-Nuñez et al., 2019*; *Döhner et al., 2021*; *Ojala et al., 2000*; *Rode et al., 2011*). In uninfected cells, there is a low amount of constitutively expressed MxB localized at the NPCs (*Crameri et al., 2018*; *Kane et al., 2018*; *Melén and Julkunen, 1997*), which might dislodge the portal cap and open the capsid portal on the incoming capsid to release the incoming genome into the nucleoplasm.

Crameri et al., proposed that the higher amounts of IFN-induced MxB may block cytosolic capsid transport, genome uncoating at the NPCs, and/or the release of viral genomes into the nucleoplasm, which is consistent with our biochemical data demonstrating MxB binding to HSV-1 capsids (*Crameri et al., 2018*). MxB-mediated disassembly of capsids that we report here would further reduce capsid targeting to the NPCs and genome release into the nucleoplasm. Accordingly, there are fewer HSV-1 capsid puncta in MxB expressing cells (*Crameri et al., 2018*). Consistent with our data on capsid disassembly with MxB(26-715), MxB(K131A), or MxB(M574D), restricting the infection of HSV-1, MCMV, and MHV68 also requires the NTE, GTP hydrolysis, and dimerization of MxB (*Crameri et al., 2018*; *Schilling et al., 2018*). Restriction of HIV infection depends also on MxB NTE and on MxB dimerization, while the role of its GTPase function requires further investigation (*Buffone et al., 2015*; *Fricke et al., 2014*; *Goujon et al., 2014*; *Schulte et al., 2015*; *Xie et al., 2021*). It will be interesting to determine whether MxB only competes for the binding of

host factors required for HIV intracellular trafficking, such as microtubule motor adaptors (BICD2; FEZ-1) or nucleoporins (reviewed in *Temple et al., 2020*), or whether it also induces HIV capsid disassembly.

Our data together with Schilling et al., and Crameri et al., suggest that the IFN-inducible MxB restricts HSV-1, HSV-2, VZV, and possibly other herpesviruses, by promoting efficient capsid disassembly (*Schilling et al., 2018*; *Crameri et al., 2018*). We cannot exclude that a surplus of capsid- and NPC-associated MxB imposes further restrictions on intracellular transport and genome release into the nucleoplasm. However, if MxB(1-715) would disassemble viral capsids before they are oriented properly with their portal toward the NPCs, their genomes would end up in the cytosol and would not be delivered into the nucleoplasm. There are fewer incoming cytoplasmic capsids in cells expressing MxB (*Crameri et al., 2018*), and incoming VP5 is ubiquitinated and degraded by proteasomes in macrophages (*Horan et al., 2013*; *Sun et al., 2019*). Therefore, capsid disassembly intermediates might be degraded in cells, while we could characterize them in our biochemical cell-free assays in which proteases had been blocked.

The viral genomes exposed after MxB-induced capsid disassembly might be degraded by the DNase TREX1 (*Sun et al., 2019*), or stimulate the DNA sensors AIM2, cGAS, or IFI16, and the induction of antiviral host mechanisms. As an inoculation with destabilized HIV-1 capsids leads to an increased activation of the DNA sensor cGAS (*Sumner et al., 2020*), the IFN-induced increased MxB expression might lead to a similar outcome in cells infected with herpesviruses. Accordingly, MxB may not only restrict herpesviruses by capsid disassembly, but also increase the exposure of viral genomes to cytosolic DNA sensors, which in turn would induce an IFN response, inflammation as well as innate and adaptive immune responses. Thus, MxB could be the long sought-after capsid sensor that destroys the sturdy herpesvirus capsids, and possibly HIV cores and other viral capsids, to promote host viral genome sensing.

Materials and methods
Cells

All cells were maintained in a humidified incubator at 37 °C with 5% CO_2, passaged twice per week, and were tested negative for mycoplasma contamination. BHK-21 (ATCC CCL-10) and Vero cells (ATCC CCL-81) were cultured in MEM Eagle with 1% NEAA (Cytogen, Wetzlar, Germany) and 10% or 7.5% (v/v) FBS, respectively (Good Forte; PAN-Biotech, Aidenbach, Germany). HaCat (*Boukamp et al., 1988*; kind gift from Detlef Neumann, Hannover Medical School, Hannover, Germany) and hTERT RPE-1 (RPE; CRL-2302, Clontech) were cultured in DMEM Gibco (Invitrogen) with 7.5% or 10% (v/v) FBS, respectively (Capricorn Scientific, Ebsdorfergrund, Germany). THP-1 cells (ATCC TIB-202; kind gift from Walther Mothes, Yale University, New Haven, USA) were cultured in RPMI Medium 1640 (Thermo Fisher Scientific, Waltham, Massachusetts, United States) with 10% FBS (Thermo Fisher Scientific, Waltham, Massachusetts, United States). THP-1 were stimulated with 100 nM phorbol 12-myristate 13-acetate (PMA; Sigma-Aldrich, Germany) for 48 hr and used immediately (Mφ) or after 3 days of rest (Mφ$_R$). The cells were cultured with 1000 U/mL human type I IFN-α2a (Mφ$_{IFN}$; R&D Systems, Minneapolis, Minnesota, USA) or left untreated for 16 hr.

A549-derived cells (ATCC CCL-185) were cultured in DMEM with 10% FCS. In addition to A549 control cells, we used A549 cell lines stably expressing MxB(1-715), MxB(1–715/K131A), MxB(1–715/T151A), MxB(1–715/M574D), MxB(26-715), or MxA(1-662) upon transduction with the respective pLVX vectors with an engineered Kozak sequence to favor expression of the MxB(1-715) over the MxB(26-715) proteins (*Schilling et al., 2018*). Furthermore, we generated A549-MxBFLAG cells expressing MxB(1-715)FLAG and MxB(26-715)FLAG, both tagged with the FLAG epitope (GACTACAAAGACGATGACGACAAG) at the C-terminus of MxB (GenBAnk NM_002463), and A549-MxB(1-715)-MxB(26-715) cells expressing untagged MxB(1-715) and MxB(26-715) using the pLKOD-Ires-Puro vector (Clontech Takara Bio, Mountain View, United States). MeWo cells (kind gift from Graham Ogg; University of Oxford, Oxford, UK) were cultured in MEM with 10% FCS, NEAA, and 1 mM sodium pyruvate. None of the cells used in this study were identified in the list of commonly misidentified cell lines (International Cell Line Authentication Committee; https://iclac.org).

Viruses

Virus stocks of HSV-1(17$^+$)Lox (*Sandbaumhüter et al., 2013*), HSV-1 strain KOS (*Warner et al., 1998*; kind gift from Pat Spear, Northwestern Medical School, Chicago, USA), and HSV-2 strain 333 (*Warner et al., 1998*; kind gift from Helena Browne, Cambridge University, Cambridge, UK) were prepared as reported before (*Döhner et al., 2006*, *Grosche et al., 2019*). Extracellular particles were harvested from the supernatant of BHK-21 cells infected with 3–4 x 10^4 PFU/mL (MOI of 0.01 PFU/cell) for 2–3 days until the cells had detached from the culture flasks, and plaque-titrated on Vero cells. VZV rOka (kind gift from Jeffrey Cohen, NIH, Bethesda, US) was maintained in infected MeWo cells (*Cohen and Seidel, 1993*; *Hertzog et al., 2020*). After 2–4 days, the VZV-infected cells as indicated by cytopathic effects were harvested, mixed with naive MeWo cells at a ratio of 1:4 to 1:8 for continued culture. Aliquots of frozen infected cells were used to inoculate cultures used for capsid preparation.

HSV-1 infection

THP-1 were seeded at 2.5×10^5 cells per six-well, treated with 100 nM PMA (Sigma-Aldrich, Germany) for 48 hr, and used immediately (Mφ) or after 3 days of rest (Mφ$_R$). The cells were then induced with 1000 U/mL of IFN-α (Mφ$_{IFN}$) or left untreated for 16 hr. On the next day, they were inoculated with HSV-1(17$^+$)Lox at 2.5×10^6, 2.5×10^7, or 5×10^7 PFU/mL (MOI of 5, 50, or 100 respectively) in CO$_2$-independent medium (Gibco Life Technologies) supplemented with 0.1% (w/v) cell culture grade fatty-acid-free bovine serum albumin (BSA; PAA Laboratories GmbH) for 30 min, and then shifted to regular culture medium at 37 °C and 5% CO$_2$. At the indicated times, the cells and the corresponding media were harvested separately and snap-frozen in liquid nitrogen. These samples as well as and HSV-1 and HSV-2 inocula were titrated on Vero cells (*Döhner et al., 2006*, *Grosche et al., 2019*).

Preparation of $V_{0.1}$, $V_{0.5}$, and V_1 and D capsids

Extracellular HSV-1 or HSV-2 particles were harvested by sedimentation at 12,000 rpm for 90 min at 4 °C (Type 19 rotor, Beckman-Coulter) from the medium of BHK-21 cells (40 × 175 cm² flasks; 2–2.5 x 10^7 cells/flask) infected with 0.01 PFU/cell (2–6.7 x 10^4 PFU/mL) for 2.5 days. The resulting medium pellets (MP) were resuspended in 2 mL of MKT buffer (20 mM MES, 30 mM Tris-HCl, 100 mM KCl, pH 7.4), treated with 0.5 mg/mL trypsin (Sigma-Aldrich, Germany) at 37 °C for 1 hr which was then inactivated with 5 mg/mL trypsin inhibitor from soybean (SBTI; Fluka, Switzerland) for 10 min on ice (*Ojala et al., 2000*; *Radtke et al., 2010*; *Radtke et al., 2014*; *Wolfstein et al., 2006*. These samples were then mixed with an equal volume of 2-fold lysis buffer (2% TX-100, 20 mM MES, 30 mM Tris, pH 7.4, 20 mM DTT, 1 x protease inhibitor cocktail [PIs, Roche cOmplete] with 0.2 M, 1 M or 2 M KCl; *Radtke et al., 2014*). The samples were layered on top of 20% (w/v) sucrose cushions in 20 mM MES, 30 mM Tris, pH 7.4 with 10 mM DTT, PIs with the respective KCl concentration, and sedimented at 110,000 g for 20 min at 4 °C (TLA-120.2 rotor, Beckman-Coulter). The supernatants and the cushions containing solubilized viral envelope and tegument proteins were carefully removed. The pellets were resuspended in BRB80 (80 mM PIPES, pH 6.8, 12 mM MgCl$_2$, 1 mM EGTA) with 10 mM DTT, PIs, 0.1 U/mL protease-free DNase I (Promega, USA), and 100 mg/mL protease-free RNase (Roth GmbH, Germany) for 1 hr at 37 °C and then overnight at 4 °C. The capsids were sedimented at 110,000 g for 15 min at 4 °C (TLA-120.2) and resuspended in capsid binding buffer (CBB: 5% [w/v] sucrose, 20 mM HEPES-KOH, pH 7.3, 80 mM K-acetate, 1 mM EGTA, 2 mM Mg-acetate, 10 mM DTT and PIs) by ultrasound tip sonication at 40 W for about 5 × 5 s on ice. Furthermore, we treated $V_{0.1}$ capsids for 40 min at 37 °C with 10 μg/mL trypsin in CBB lacking PIs to generate D capsids by limited digestion. After the addition of 5 mg/mL SBTI for 10 min on ice to block the trypsin activity, the D capsids were sedimented at 110,000 x g and 4 °C for 15 min (TLA-120.2), and resuspended in CBB with PIs.

Preparation of nuclear A, B, and C capsids

HSV-1 nuclear capsids were prepared from 40 × 175 cm² flasks with BHK-21 cells infected with 0.01 PFU/cell (3–4 x 10^4 PFU/mL) for about 2.5 days (*Anderson et al., 2014*; *Radtke et al., 2010*; *Radtke et al., 2014*; *Snijder et al., 2017*; *Wolfstein et al., 2006*). VZV nuclear capsids were harvested from infected MeWo cells cultured in 5–10 x 175 cm² flasks at maximum syncytia formation but before cell lysis. The cells were harvested, resuspended in MKT buffer (20 mM MES, 30 mM Tris, pH 7.4, 100 mM KCl), snap-frozen, and stored at –80 °C. Nuclear A, B, and C capsids were separated by sedimentation at 50,000 x g and 4 °C for 80 min (SW40Ti, Beckman Coulter) on linear 20% to 50% sucrose gradients

in TKE buffer 20 mM Tris, pH 7.5, 500 mM KCl, 1 mM EDTA; diluted in three volumes of TKE supplemented with 2 mM DTT and PIs (Roche cOmplete). The capsids were sedimented in BSA-coated centrifuge tubes at 110,000 g at 4 °C for 20 min (TLA-120.2), resuspended in BRB80 buffer supplemented with 100 mg/mL RNase (Roth, Germany), 0.1 U/mL DNase I (M6101, Promega, USA), 10 mM DTT, and PIs, sedimented again, and resuspended in CBB with PIs.

Calibration of capsid concentration

To calibrate the amount of capsid equivalents (CAP_{eq}) among different experiments, we compared all capsid preparations used in this study with a calibration curve generated from the same starting preparation. The capsids were suspended in sample buffer (1% [w/v] SDS, 50 mM Tris-HCl, pH 6.8, 1% [v/v] β-mercaptoethanol, 5% [v/v] glycerol, PIs [Roche cOmplete]), and adsorbed to nitrocellulose membranes (BioTrace, Pall Laboratory) using a 48-slot suction device (Bio-DOT-SF, Bio-Rad, Hercules, California, USA). The membranes were probed with a polyclonal rabbit serum raised against purified HSV-1 nuclear capsids (SY4563; *Supplementary file 4*; *Döhner et al., 2018*) followed by secondary antibodies conjugated to fluorescent infrared dyes (donkey-anti-rabbit IgG-IRDye1 800CW; *Supplementary file 3*), and documented with an Infrared Imaging System (Odyssey, Image Studio Lite Quantification Software, LI-COR Biosciences, Lincoln, Nebraska, USA). MPs harvested from one 175 cm² flasks of BHK-21 cells infected with HSV-1 contained about $0.5–1 \times 10^9$ PFU/mL, and $0.75–1.5 \times 10^9$ CAP_{eq}/mL. A nuclear HSV-1 capsid fraction prepared from one 175 cm² flask contained about $0.5–1 \times 10^7$ CAP_{eq} of A capsids, $1–2 \times 10^7$ CAP_{eq} of B capsids, and $0.5–0.75 \times 10^7$ CAP_{eq} of C capsids, and a nuclear VZV fraction from one 175 cm² flasks of MeWo cells $2–4 \times 10^5$ CAP_{eq} of A capsids, $0.5–1 \times 10^6$ CAP_{eq} of B capsids, and $0.8–1.6 \times 10^7$ CAP_{eq} of C capsids. Capsid-host protein complexes were assembled *in-solution* using 7.5×10^8 CAP_{eq}/condition for MS and immunoblot experiments, and for the *on-grid* electron microscopy assay 2×10^7 CAP_{eq}/condition were used.

Preparation of cytosol

Cytosolic extracts were prepared as described before (*Radtke et al., 2010*; *Radtke et al., 2014*), dialyzed (7 K MW cut-off cassettes; Slide-A-Lyzer, Thermo Scientific), snap-frozen and stored at –80 °C. Prior to their use, the cytosols were supplemented with 1 mM ATP, 1 mM GTP, 7 mM creatine phosphate, 5 mM DTT, and PIs (Roche cOmplete), and centrifuged at 130,000 g for 30 min at 4 °C (TLA-120.2). We added nocodazole to 25 µM to the cytosols, and left them either untreated (ATP/GTP^{high}) or supplemented them with 10 U/mL apyrase (Sigma; ATP/GTP^{low}) for 15 min at RT.

Assembly of capsid-host protein complexes *in-solution*

Capsids were resuspended in CBB and cytosol at a protein concentration of 0.2 mg/mL in an assay volume of 60 µL per sample on a rotating platform at 800 rpm for 1 hr at 37 °C (c.f. *Figure 2—figure supplement 1*). The capsid-host protein complexes were sedimented through a 30% sucrose cushion at 110,000 g for 20 min at 4 °C (TLA-100, Beckman-Coulter), resuspended in CBB by ultrasound tip sonication at 40 W for about 5×5 s on ice, and analyzed by mass spectrometry, immunoblot, or electron microscopy (*Radtke et al., 2014*).

SDS-PAGE and immunoblot

The samples were lysed in Laemmli buffer (1% [w/v] SDS, 50 mM Tris-HCl, pH 6.8, 1% [v/v] β-mercaptoethanol, 5% [v/v] glycerol, bromophenol blue, PIs [Roche cOmplete]). The proteins were separated on linear 7.5% to 12% or 10% to 15% SDS-PAGE, transferred to methanol-activated PVDF membranes, probed with rabbit or murine primary antibodies (*Supplementary file 3*) and secondary antibodies conjugated to fluorescent infrared dyes (anti-rabbit IgG-IRDye1 800CW; anti-mouse IgG-IRDye1 680RD; *Supplementary file 3*) and documented with an Infrared Imaging System (Odyssey, Image Studio Lite Quantification Software, LI-COR Biosciences, Lincoln, Nebraska, USA).

Mass spectrometry sample preparation and measurement

Capsid-host protein complexes were analyzed by liquid chromatography coupled to tandem mass spectrometry (LC-MS/MS) in four independent biological replicates. The samples were resuspended in hot Laemmli buffer and separated in NuPAGE 4% to 12% Bis-Tris protein gels (Invitrogen) before *in*-gel digestion. Briefly, proteins were fixed and stained by Coomassie solution (0.4% G250, 30%

methanol, 10% acetic acid). Sample lanes were excised, destained (50% ethanol, 25 mM ammonium bi-carbonate), dehydrated with 100% ethanol and dried using a SpeedVac centrifuge (Eppendorf, Concentrator plus). Gel pieces were rehydrated in trypsin solution (1/50 [w/w] trypsin/protein) overnight at 37 °C. Tryptic peptides were extracted in extraction buffer (3% trifluoroacetic acid, 30% acetonitrile), dried using a SpeedVac centrifuge, resuspended in 2 M Tris-HCl buffer before reduction and alkylation using 10 mM Tris(2-carboxyethyl)phosphine, 40 mM 2-Chloroacetamide in 25 mM Tris-HCl pH 8.5. The peptides were purified, concentrated on StageTips with three C18 Empore filter discs (3 M), separated on a liquid chromatography instrument, and analyzed by mass spectrometry (EASY- nLC 1200 system on an LTQ-Orbitrap XL; Thermo Fisher Scientific) as described before (*Hubel et al., 2019*). Peptides were loaded on a 20 cm reverse-phase analytical column (75 μm column diameter; ReproSil-Pur C18-AQ 1.9 μm resin; Dr. Maisch) and separated using a 120 min acetonitrile gradient. The mass spectrometer was operated in Data-Dependent Analysis mode (DDA, XCalibur software v.3.0, Thermo Fisher).

Mass-spectrometry data analysis

Raw files were processed with MaxQuant using iBAQ quantification and Match Between Runs option, and the protein groups were filtered with Perseus for reverse identification, modification site only identification, and MaxQuant contaminant list (https://maxquant.net/maxquant/, v1.6.2.10; https://maxquant.net/perseus/, v1.6.5.0; *Cox and Mann, 2008*; *Tyanova et al., 2016a*; *Tyanova et al., 2016b*). The iBAQ intensities were normalized across all samples to the overall median intensity of the HSV-1 capsid protein VP5. Cytosol and beads incubated with cytosol samples were normalized to all proteins detected in at least three replicates in each condition. Significant differences between given conditions were determined by a two-sided Welch t-test on protein groups present in three replicates of at least one condition, followed by permutation-based FDR statistics (250 permutations), using an absolute $\log_2$ difference cut-off of 1 and an FDR cut-off of 0.05. To characterize the IFN induction, we annotated proteins reported as being induced by IFN type-I as *ISGs* proteins (InterferomeDB, > 2 x change; http://www.interferome.org/interferome/home.jspx; *Rusinova et al., 2013*). We used the Fisher's exact test against *ISGs* proteins as well as all Gene Ontology terms (GO; *Ashburner et al., 2000*; *Consortium, 2021*; http://geneontology.org/) for enrichment analysis of proteins upregulated in IFN-induced Mφ$_{IFN}$ cytosol over Mφ$_R$ cytosol ($\log_2$ difference ≥1.5; permutation-based FDR ≤ 0.05). The data were summarized in volcano or bar plots (GraphPad Prism v5.0, https://www.graphpad.com/; Perseus v1.6.5.0; *Tyanova et al., 2016b*).

Interaction network assembly

We focused our analysis on proteins that showed specific differences from one capsid preparation to the other, within the same cytosol preparation, and considered host proteins with an enrichment higher than 1.5 $\log_2$ fold changes and a permutation-based FDR ≤ 0.01 as specifically enriched. To visualize enrichment among different capsid-host protein complexes, we generated integrative networks using Cytoscape (http://www.cytoscape.org/; v3.7.2; *Shannon et al., 2003*) and STRING (confidence score: 0.7; *Szklarczyk et al., 2019*). STRING uses a combination of databases on co-expression, conserved occurrences, GO terms and Kyoto Encyclopedia of Genes and Genomes (KEGG; https://www.genome.jp/kegg/; *Kanehisa and Goto, 2000*; *Kanehisa, 2019*; *Kanehisa et al., 2021*). To assemble pathway enrichments, we used DAVID, a Database for Annotation, Visualization and Integrated Discovery (https://david.ncifcrf.gov/home.jsp; v6.8; *Huang et al., 2009a*; *Huang et al., 2009b*) and the Cytoscape plug-ins ClueGO and CluePedia (http://apps.cytoscape.org/apps/cluego, v2.5.7; http://apps.cytoscape.org/apps/cluepedia, v1.5.7; *Bindea et al., 2009*; *Bindea et al., 2013*).

Electron microscopy

Capsid-host protein complexes were assembled at ATP/GTP^{high} in solution, harvested by ultracentrifugation, resuspended in CBB, and adsorbed onto enhanced hydrophilicity-400 mesh formvar- and carbon-coated copper grids (Stork Veco, The Netherlands; *Radtke et al., 2010*; *Roos et al., 2009*). Moreover, capsids at a concentration of 1 × 10⁷ CAP$_{eq}$/mL were adsorbed directly for 20 min at RT onto the grids. The grids were incubated on a 10 μL drop of cytosol with a protein concentration of 0.2 mg/mL and ATP/GTP^{high} in a humid chamber for 1 hr at 37 °C. The samples were left untreated or labeled with anti-VP5 (pAb NC-1) and protein-A gold (10 nm diameter; Cell Microscopy Centre,

Utrecht School of Medicine, The Netherlands). For both protocols, the grids were washed with PBS and ddH$_2$O, contrasted with 2% uranyl acetate at pH 4.4, air dried, and analyzed by transmission electron microscopy (Morgani or Tecnai; FEI, Einthoven, The Netherlands). The capsid morphology was evaluated for about 100 structures/assay from about 15 randomly selected images of 2.7 μm² of three biological replicates. We classified capsomer-containing structures as *punched*, if they lacked one or more of their vertices but still had an icosahedral shape, and as *flat shells*, if they lacked the icosahedral shape but contained capsomers, and scored them as one capsid equivalent structure if they contained more than 100 capsomers.

Capsid DNA uncoating assay

D capsids were incubated with cytosols from A549-control, A549-MxB(1-715), A549-MxB(M574D), or A549-MxB-FLAG for 1 hr at 37 °C or treated for 5 min with 1% SDS followed by 10 min with 10% TX-100 (*Ojala et al., 2000*). The viral genomes released during the assay were degraded by adding 50 U/mL of benzonase for 1 hr at 37 °C, and the remaining protected DNA was purified with the DNA Blood Mini Kit (Qiagen, Hilden, Germany) and quantified by real-time PCR on a qTower³ (Analytik Jena, Jena, Germany). The SYBR Green assay was performed with the Luna Universal qPCR Master Mix (NEB, Ipswich, MA, USA) according to the manufacturer's instructions with primers specific for HSV-1 gB (UL27 gene) (HSV1_2 SYBR fwd: 5′-gtagccgtaaaacggggaca-3′ and HSV1_2 SYBR rev: 5′-ccgacctc aagtacaacccc-3′; *Engelmann et al., 2008*). Standards and samples were run in triplicates and results expressed as % released viral DNA with the SDS/Tx-100 treatment normalized to 100%.

Quantification and statistical analyses

We performed Welch's t-testing, Kruskal-Wallis H-testing, Friedman and one-way analyses of variance with a Dunns or Bonferroni post-testing (GraphPad Prism v5.0; https://www.graphpad.com/).

Acknowledgements

Additional information

Author contributions

Author ORCIDs

Manutea C Serrero http://orcid.org/0000-0001-8221-2725
Jonny Hertzog http://orcid.org/0000-0002-7089-982X
Andreas Pichlmair http://orcid.org/0000-0002-0166-1367
Beate Sodeik http://orcid.org/0000-0003-4650-3036

Decision letter and Author response

Decision letter https://doi.org/10.7554/eLife.76804.sa1
Author response https://doi.org/10.7554/eLife.76804.sa2

Additional files

Supplementary files

• Supplementary file 1. Host proteins in THP-1 cytosols. Intensity-Based Absolute Quantitation (iBAQ) counts of the host proteins identified in the proteomic analysis of the cytosolic extracts prepared from rested or IFN-induced THP-1 φ cytosol. Statistical analyses were performed with a Welch's t-test. The following cut-offs were set for differentially-expressed proteins: permutation-based false-discovery rate (FDR) ≤ 0.05 and $|\log_2 \text{ fold-change}| \geq 1.5$. The protein groups were filtered to keep only the intensities measured in at least three out of four replicates per condition. Gene Ontology knowledge was used to reference the proteins previously described as induced by interferon.

• Supplementary file 2. Host proteins in capsid-host protein complexes. Intensity-Based Absolute Quantitation (iBAQ) counts of host proteins identified in the $V_{0.1}$, $V_{0.5}$, V_1 and D capsid-host protein complexes assembled in rested or IFN-induced THP-1 φ cytosol. Statistical analyses were performed with a Welch's t-test. The following cut-offs were set for differentially bound proteins: permutation-based false-discovery rate (FDR) ≤ 0.05 and a $|\log_2 \text{ fold-change} \geq 1.5|$. The protein groups were filtered to keep only those with intensities measured in at least three out of four replicates, in at least one condition. "Interaction significance" column indicates the proteins considered as specific interactors.

• Supplementary file 3. Viral proteins in capsid-host protein complexes. Intensity-based absolute quantification (iBAQ) counts of HSV-1(17$^+$)Lox viral proteins from isolated $V_{0.1}$, $V_{0.5}$, V_1 and D capsids (A) normalized to the intensity of the major capsid protein VP5, (B) unnormalized LFQ intensities. The viral proteins were filtered to keep only those with intensities measured in at least three out of four replicates, in at least one condition.

• Supplementary file 4. List of Antibodies. mAb: monoclonal antibody. pAb: polyclonal antibody. Anti-capsid SY4563 (*Döhner et al., 2018*); Anti-VP5 NC-1 (*Cohen et al., 1980*); anti-calnexin (*Hammond and Helenius, 1994*); Anti-MxA/MxB M143 (*Flohr et al., 1999*).

• Transparent reporting form

Data availability

The raw datasets produced in this study are available at PRIDE (PXD028276; http://www.ebi.ac.uk/pride). The dataset analyses and the raw bottling images are included in the Supplementary Files 1-3 and in the Source Data folder, respectively.

The following dataset was generated:

Author(s)	Year	Dataset title	Dataset URL	Database and Identifier
Serrero MC, Girault V, Pichlmair A, Sodeik B	2021	The interferon-inducible antiviral GTPase MxB promotes capsid disassembly and genome release of herpesviruses	https://www.ebi.ac.uk/pride/archive/projects/PXD028276	PRIDE, PXD028276

References

Alvarez FJD, He S, Perilla JR, Jang S, Schulten K, Engelman AN, Scheres SHW, Zhang P. 2017. CryoEM structure of MxB reveals a novel oligomerization interface critical for HIV restriction. *Science Advances* **3**:e1701264. DOI: https://doi.org/10.1126/sciadv.1701264, PMID: 28929138

Anderson F, Savulescu AF, Rudolph K, Schipke J, Cohen I, Ibiricu I, Rotem A, Grünewald K, Sodeik B, Harel A. 2014. Targeting of viral capsids to nuclear pores in a cell-free reconstitution system. *Traffic* **15**:1266–1281. DOI: https://doi.org/10.1111/tra.12209, PMID: 25131140

Arvin AM, Abendroth A. 2021. Varicella–Zoster Virus. Howley PM, Knipe DM, Cohen JL, Damania BA (Eds). *Fields Virology: DNA Viruses*. Wolters Kluwer Health/Lippincott Williams & Wilkins. p. 445–488.

Ashburner M, Ball CA, Blake JA, Botstein D, Butler H, Cherry JM, Davis AP, Dolinski K, Dwight SS, Eppig JT, Harris MA, Hill DP, Issel-Tarver L, Kasarskis A, Lewis S, Matese JC, Richardson JE, Ringwald M, Rubin GM, Sherlock G. 2000. Gene Ontology: tool for the unification of biology. *Nature Genetics* **25**:25–29. DOI: https://doi.org/10.1038/75556

Bauer DW, Huffman JB, Homa FL, Evilevitch A. 2013. Herpes virus genome, the pressure is on. *Journal of the American Chemical Society* **135**:11216–11221. DOI: https://doi.org/10.1021/ja404008r, PMID: 23829592

Betancor G, Dicks MDJ, Jimenez-Guardeño JM, Ali NH, Apolonia L, Malim MH. 2019. The GTPase Domain of MX2 Interacts with the HIV-1 Capsid, Enabling Its Short Isoform to Moderate Antiviral Restriction. *Cell Reports* **29**:1923-1933.. DOI: https://doi.org/10.1016/j.celrep.2019.10.009, PMID: 31722207

Bindea G, Mlecnik B, Hackl H, Charoentong P, Tosolini M, Kirilovsky A, Fridman WH, Pagès F, Trajanoski Z, Galon J. 2009. ClueGO: a Cytoscape plug-in to decipher functionally grouped gene ontology and pathway annotation networks. *Bioinformatics* **25**:1091–1093. DOI: https://doi.org/10.1093/bioinformatics/btp101, PMID: 19237447

Bindea G, Galon J, Mlecnik B. 2013. CluePedia Cytoscape plugin: pathway insights using integrated experimental and in silico data. *Bioinformatics* **29**:661–663. DOI: https://doi.org/10.1093/bioinformatics/btt019, PMID: 23325622

Boukamp P, Petrussevska RT, Breitkreutz D, Hornung J, Markham A, Fusenig NE. 1988. Normal keratinization in a spontaneously immortalized aneuploid human keratinocyte cell line. *The Journal of Cell Biology* **106**:761–771. DOI: https://doi.org/10.1083/jcb.106.3.761, PMID: 2450098

Brandariz-Nuñez A, Liu T, Du T, Evilevitch A. 2019. Pressure-driven release of viral genome into a host nucleus is a mechanism leading to herpes infection. *eLife* **8**:e47212. DOI: https://doi.org/10.7554/eLife.47212, PMID: 31393262

Buffone C, Schulte B, Opp S, Diaz-Griffero F. 2015. Contribution of MxB oligomerization to HIV-1 capsid binding and restriction. *Journal of Virology* **89**:3285–3294. DOI: https://doi.org/10.1128/JVI.03730-14, PMID: 25568212

Cabrera JR, Manivanh R, North BJ, Leib DA. 2019. The ESCRT-Related ATPase Vps4 Is Modulated by Interferon during Herpes Simplex Virus 1 Infection. *mBio* **10**:e02567-18. DOI: https://doi.org/10.1128/mBio.02567-18, PMID: 30837340

Cao H, Krueger EW, Chen J, Drizyte-Miller K, Schulz ME, McNiven MA. 2020. The anti-viral dynamin family member MxB participates in mitochondrial integrity. *Nature Communications* **11**:1048. DOI: https://doi.org/10.1038/s41467-020-14727-w, PMID: 32102993

Carter-Timofte ME, Paludan SR, Mogensen TH. 2018. RNA Polymerase III as a Gatekeeper to Prevent Severe VZV Infections. *Trends in Molecular Medicine* **24**:904–915. DOI: https://doi.org/10.1016/j.molmed.2018.07.009, PMID: 30115567

Chen Y, Zhang L, Graf L, Yu B, Liu Y, Kochs G, Zhao Y, Gao S. 2017. Conformational dynamics of dynamin-like MxA revealed by single-molecule FRET. *Nature Communications* **8**:15744. DOI: https://doi.org/10.1038/ncomms15744, PMID: 28548099

Cohen GH, Ponce de Leon M, Diggelmann H, Lawrence WC, Vernon SK, Eisenberg RJ. 1980. Structural analysis of the capsid polypeptides of herpes simplex virus types 1 and 2. *Journal of Virology* **34**:521–531. DOI: https://doi.org/10.1128/JVI.34.2.521-531.1980, PMID: 6154808

Cohen JI, Seidel KE. 1993. Generation of varicella-zoster virus (VZV) and viral mutants from cosmid DNAs: VZV thymidylate synthetase is not essential for replication in vitro. *PNAS* **90**:7376–7380. DOI: https://doi.org/10.1073/pnas.90.15.7376, PMID: 8394020

Coller KE, Lee JI-H, Ueda A, Smith GA. 2007. The capsid and tegument of the alphaherpesviruses are linked by an interaction between the UL25 and VP1/2 proteins. *Journal of Virology* **81**:11790–11797. DOI: https://doi.org/10.1128/JVI.01113-07, PMID: 17715218

Consortium GO. 2021. The Gene Ontology resource: enriching a GOld mine. *Nucleic Acids Research* **49**:D325–D334. DOI: https://doi.org/10.1093/nar/gkaa1113, PMID: 33290552

Cox J, Mann M. 2008. MaxQuant enables high peptide identification rates, individualized p.p.b.-range mass accuracies and proteome-wide protein quantification. *Nature Biotechnology* **26**:1367–1372. DOI: https://doi.org/10.1038/nbt.1511, PMID: 19029910

Crameri M, Bauer M, Caduff N, Walker R, Steiner F, Franzoso FD, Gujer C, Boucke K, Kucera T, Zbinden A, Münz C, Fraefel C, Greber UF, Pavlovic J. 2018. MxB is an interferon-induced restriction factor of human herpesviruses. *Nature Communications* **9**:1980–1982. DOI: https://doi.org/10.1038/s41467-018-04379-2, PMID: 29773792

Crump CM, Yates C, Minson T. 2007. Herpes simplex virus type 1 cytoplasmic envelopment requires functional Vps4. *Journal of Virology* **81**:7380–7387. DOI: https://doi.org/10.1128/JVI.00222-07, PMID: 17507493

Crump CM. 2018. Virus Assembly and Egress of HSV. *Advances in Experimental Medicine and Biology* **1045**:23–44. DOI: https://doi.org/10.1007/978-981-10-7230-7_2, PMID: 29896661

Dai X, Zhou ZH. 2018. Structure of the herpes simplex virus 1 capsid with associated tegument protein complexes. *Science* **360**:eaao7298. DOI: https://doi.org/10.1126/science.aao7298, PMID: 29622628

Diefenbach RJ. 2015. Conserved tegument protein complexes: Essential components in the assembly of herpesviruses. *Virus Research* **210**:308–317. DOI: https://doi.org/10.1016/j.virusres.2015.09.007, PMID: 26365681

Döhner K, Radtke K, Schmidt S, Sodeik B. 2006. Eclipse phase of herpes simplex virus type 1 infection: Efficient dynein-mediated capsid transport without the small capsid protein VP26. *Journal of Virology* **80**:8211–8224. DOI: https://doi.org/10.1128/JVI.02528-05, PMID: 16873277

Döhner K, Ramos-Nascimento A, Bialy D, Anderson F, Hickford-Martinez A, Rother F, Koithan T, Rudolph K, Buch A, Prank U, Binz A, Hügel S, Lebbink RJ, Hoeben RC, Hartmann E, Bader M, Bauerfeind R, Sodeik B, Hutt-Fletcher L. 2018. Importin α1 is required for nuclear import of herpes simplex virus proteins and capsid assembly in fibroblasts and neurons. *PLOS Pathogens* **14**:e1006823. DOI: https://doi.org/10.1371/journal.ppat.1006823, PMID: 29304174

Döhner K, Cornelius A, Serrero MC, Sodeik B. 2021. Herpesvirus Capsids on Their Journey to the Center of the Cell. *Current Opinion in Virology* **50**:147–158. DOI: https://doi.org/10.1016/j.coviro.2021.08.005, PMID: 34464845

Engelmann I, Petzold DR, Kosinska A, Hepkema BG, Schulz TF, Heim A. 2008. Rapid quantitative PCR assays for the simultaneous detection of herpes simplex virus, varicella zoster virus, cytomegalovirus, Epstein-Barr virus, and human herpesvirus 6 DNA in blood and other clinical specimens. *Journal of Medical Virology* **80**:467–477. DOI: https://doi.org/10.1002/jmv.21095, PMID: 18205230

Everett RD, Meredith M, Orr A, Cross A, Kathoria M, Parkinson J. 1997. A novel ubiquitin-specific protease is dynamically associated with the PML nuclear domain and binds to A herpesvirus regulatory protein. *The EMBO Journal* **16**:566–577. DOI: https://doi.org/10.1093/emboj/16.3.566, PMID: 9034339

Flohr F, Schneider-Schaulies S, Haller O, Kochs G. 1999. The central interactive region of human MxA GTPase is involved in GTPase activation and interaction with viral target structures. *FEBS Letters* **463**:24–28. DOI: https://doi.org/10.1016/S0014-5793(99)01598-7, PMID: 10601631

Fribourgh JL, Nguyen HC, Matreyek KA, Alvarez FJD, Summers BJ, Dewdney TG, Aiken C, Zhang P, Engelman A, Xiong Y. 2014. Structural insight into HIV-1 restriction by MxB. *Cell Host & Microbe* **16**:627–638. DOI: https://doi.org/10.1016/j.chom.2014.09.021, PMID: 25312384

Fricke T, White TE, Schulte B, de Souza Aranha Vieira DA, Dharan A, Campbell EM, Brandariz-Nuñez A, Diaz-Griffero F. 2014. MxB binds to the HIV-1 core and prevents the uncoating process of HIV-1. *Retrovirology* **11**:68. DOI: https://doi.org/10.1186/s12977-014-0068-x, PMID: 25123063

Gao S, von der Malsburg A, Dick A, Faelber K, Schröder GF, Haller O, Kochs G, Daumke O. 2011. Structure of myxovirus resistance protein a reveals intra- and intermolecular domain interactions required for the antiviral function. *Immunity* **35**:514–525. DOI: https://doi.org/10.1016/j.immuni.2011.07.012, PMID: 21962493

Gershon AA, Breuer J, Cohen JI, Cohrs RJ, Gershon MD, Gilden D, Grose C, Hambleton S, Kennedy PGE, Oxman MN, Seward JF, Yamanishi K. 2015. Varicella zoster virus infection. *Nature Reviews. Disease Primers* **1**:15016. DOI: https://doi.org/10.1038/nrdp.2015.16, PMID: 27188665

Goujon C, Moncorgé O, Bauby H, Doyle T, Ward CC, Schaller T, Hué S, Barclay WS, Schulz R, Malim MH. 2013. Human MX2 is an interferon-induced post-entry inhibitor of HIV-1 infection. *Nature* **502**:559–562. DOI: https://doi.org/10.1038/nature12542, PMID: 24048477

Goujon C, Moncorgé O, Bauby H, Doyle T, Barclay WS, Malim MH. 2014. Transfer of the amino-terminal nuclear envelope targeting domain of human MX2 converts MX1 into an HIV-1 resistance factor. *Journal of Virology* **88**:9017–9026. DOI: https://doi.org/10.1128/JVI.01269-14, PMID: 24899177

Grosche L, Döhner K, Düthorn A, Hickford-Martinez A, Steinkasserer A, Sodeik B. 2019. Herpes Simplex Virus Type 1 Propagation, Titration and Single-step Growth Curves. *Bio-Protocol* **9**:e3441. DOI: https://doi.org/10.21769/BioProtoc.3441, PMID: 33654936

Haller O, Staeheli P, Schwemmle M, Kochs G. 2015. Mx GTPases: dynamin-like antiviral machines of innate immunity. *Trends in Microbiology* **23**:154–163. DOI: https://doi.org/10.1016/j.tim.2014.12.003, PMID: 25572883

Hammond C, Helenius A. 1994. Quality control in the secretory pathway: retention of a misfolded viral membrane glycoprotein involves cycling between the ER, intermediate compartment, and Golgi apparatus. *The Journal of Cell Biology* **126**:41–52. DOI: https://doi.org/10.1083/jcb.126.1.41, PMID: 8027184

Hertzog J, Rehwinkel J. 2020. Regulation and inhibition of the DNA sensor cGAS. *EMBO Reports* **21**:e51345. DOI: https://doi.org/10.15252/embr.202051345, PMID: 33155371

Hertzog J, Zhou W, Rigby RE, Fowler G, Cursi C, Chauveau L, Davenne T, Kranzusch PJ, Rehwinkel J. 2020. Varicella-Zoster Virus ORF9 Is an Antagonist of the DNA Sensor CGAS. [bioRxiv]. DOI: https://doi.org/10.1101/2020.02.11.943415

Horan KA, Hansen K, Jakobsen MR, Holm CK, Søby S, Unterholzner L, Thompson M, West JA, Iversen MB, Rasmussen SB, Ellermann-Eriksen S, Kurt-Jones E, Landolfo S, Damania B, Melchjorsen J, Bowie AG, Fitzgerald KA, Paludan SR. 2013. Proteasomal degradation of herpes simplex virus capsids in macrophages releases DNA to the cytosol for recognition by DNA sensors. *Journal of Immunology* **190**:2311–2319. DOI: https://doi.org/10.4049/jimmunol.1202749, PMID: 23345332

Huang DW, Sherman BT, Lempicki RA. 2009a. Bioinformatics enrichment tools: paths toward the comprehensive functional analysis of large gene lists. *Nucleic Acids Research* **37**:1–13. DOI: https://doi.org/10.1093/nar/gkn923, PMID: 19033363

Huang DW, Sherman BT, Lempicki RA. 2009b. Systematic and integrative analysis of large gene lists using DAVID bioinformatics resources. *Nature Protocols* **4**:44–57. DOI: https://doi.org/10.1038/nprot.2008.211, PMID: 19131956

Hubel P, Urban C, Bergant V, Schneider WM, Knauer B, Stukalov A, Scaturro P, Mann A, Brunotte L, Hoffmann HH, Schoggins JW, Schwemmle M, Mann M, Rice CM, Pichlmair A. 2019. A protein-interaction network of interferon-stimulated genes extends the innate immune system landscape. *Nature Immunology* **20**:493–502. DOI: https://doi.org/10.1038/s41590-019-0323-3, PMID: 30833792

Huffmaster NJ, Sollars PJ, Richards AL, Pickard GE, Smith GA. 2015. Dynamic ubiquitination drives herpesvirus neuroinvasion. *PNAS* **112**:12818–12823. DOI: https://doi.org/10.1073/pnas.1512559112, PMID: 26407585

Jaguva Vasudevan AA, Bähr A, Grothmann R, Singer A, Häussinger D, Zimmermann A, Münk C. 2018. MXB inhibits murine cytomegalovirus. *Virology* **522**:158–167. DOI: https://doi.org/10.1016/j.virol.2018.07.017, PMID: 30032029

Justice JL, Kennedy MA, Hutton JE, Liu D, Song B, Phelan B, Cristea IM. 2021. Systematic profiling of protein complex dynamics reveals DNA-PK phosphorylation of IFI16 en route to herpesvirus immunity. *Science Advances* **7**:eabg6680. DOI: https://doi.org/10.1126/sciadv.abg6680, PMID: 34144993

Kane M, Yadav SS, Bitzegeio J, Kutluay SB, Zang T, Wilson SJ, Schoggins JW, Rice CM, Yamashita M, Hatziioannou T, Bieniasz PD. 2013. MX2 is an interferon-induced inhibitor of HIV-1 infection. *Nature* **502**:563–566. DOI: https://doi.org/10.1038/nature12653, PMID: 24121441

Kane M, Rebensburg SV, Takata MA, Zang TM, Yamashita M, Kvaratskhelia M, Bieniasz PD. 2018. Nuclear pore heterogeneity influences HIV-1 infection and the antiviral activity of MX2. *eLife* **7**:e35738. DOI: https://doi.org/10.7554/eLife.35738, PMID: 30084827

Kanehisa M, Goto S. 2000. KEGG: kyoto encyclopedia of genes and genomes. *Nucleic Acids Research* **28**:27–30. DOI: https://doi.org/10.1093/nar/28.1.27, PMID: 10592173

Kanehisa M. 2019. Toward understanding the origin and evolution of cellular organisms. *Protein Science* **28**:1947–1951. DOI: https://doi.org/10.1002/pro.3715, PMID: 31441146

Kanehisa M, Furumichi M, Sato Y, Ishiguro-Watanabe M, Tanabe M. 2021. KEGG: integrating viruses and cellular organisms. *Nucleic Acids Research* **49**:D545–D551. DOI: https://doi.org/10.1093/nar/gkaa970, PMID: 33125081

King MC, Raposo G, Lemmon MA. 2004. Inhibition of nuclear import and cell-cycle progression by mutated forms of the dynamin-like GTPase MxB. *PNAS* **101**:8957–8962. DOI: https://doi.org/10.1073/pnas.0403167101, PMID: 15184662

Knipe DM, Heldwein EE, Mohr IJ, Sodroski CN. 2021. Herpes Simplex Viruses: Mechanisms of Lytic and Latent Infection. Howley PM, Knipe DM, Cohen JL, Damania BA (Eds). *Fields Virology: DNA Viruses*. Wolters Kluwer Health/Lippincott Williams & Wilkins. p. 235–296.

Kurt-Jones EA, Orzalli MH, Knipe DM. 2017. Innate Immune Mechanisms and Herpes Simplex Virus Infection and Disease. *Advances in Anatomy, Embryology, and Cell Biology* **223**:49–75. DOI: https://doi.org/10.1007/978-3-319-53168-7_3, PMID: 28528439

Liu SY, Sanchez DJ, Aliyari R, Lu S, Cheng G. 2012. Systematic identification of type I and type II interferon-induced antiviral factors. *PNAS* **109**:4239–4244. DOI: https://doi.org/10.1073/pnas.1114981109, PMID: 22371602

Liu Z, Pan Q, Ding S, Qian J, Xu F, Zhou J, Cen S, Guo F, Liang C. 2013. The interferon-inducible MxB protein inhibits HIV-1 infection. *Cell Host & Microbe* **14**:398–410. DOI: https://doi.org/10.1016/j.chom.2013.08.015, PMID: 24055605

Liu YT, Jiang J, Bohannon KP, Dai X, Gant Luxton GW, Hui WH, Bi GQ, Smith GA, Zhou ZH. 2017. A pUL25 dimer interfaces the pseudorabies virus capsid and tegument. *The Journal of General Virology* **98**:2837–2849. DOI: https://doi.org/10.1099/jgv.0.000903, PMID: 29035172

Liu YT, Jih J, Dai X, Bi GQ, Zhou ZH. 2019. Cryo-EM structures of herpes simplex virus type 1 portal vertex and packaged genome. *Nature* **570**:257–261. DOI: https://doi.org/10.1038/s41586-019-1248-6, PMID: 31142842

Lum KK, Cristea IM. 2021. Host Innate Immune Response and Viral Immune Evasion During Alphaherpesvirus Infection. *Current Issues in Molecular Biology* **42**:635–686. DOI: https://doi.org/10.21775/cimb.042.635, PMID: 33640867

Ma Z, Ni G, Damania B. 2018. Innate Sensing of DNA Virus Genomes. *Annual Review of Virology* **5**:341–362. DOI: https://doi.org/10.1146/annurev-virology-092917-043244, PMID: 30265633

McElwee M, Vijayakrishnan S, Rixon F, Bhella D. 2018. Structure of the herpes simplex virus portal-vertex. *PLOS Biology* **16**:e2006191. DOI: https://doi.org/10.1371/journal.pbio.2006191, PMID: 29924793

Melén K, Keskinen P, Ronni T, Sareneva T, Lounatmaa K, Julkunen I. 1996. Human MxB protein, an interferon-alpha-inducible GTPase, contains a nuclear targeting signal and is localized in the heterochromatin region beneath the nuclear envelope. *The Journal of Biological Chemistry* **271**:23478–23486. DOI: https://doi.org/10.1074/jbc.271.38.23478, PMID: 8798556

Melén K, Julkunen I. 1997. Nuclear cotransport mechanism of cytoplasmic human MxB protein. *The Journal of Biological Chemistry* **272**:32353–32359. DOI: https://doi.org/10.1074/jbc.272.51.32353, PMID: 9405443

Naniima P, Naimo E, Koch S, Curth U, Alkharsah KR, Stroh LJ, Binz A, Beneke JM, Vollmer B, Boning H, Borst EM, Desai P, Bohne J, Messerle M, Bauerfeind R, Legrand P, Sodeik B, Schulz TF, Krey T. 2021. Assembly of infectious Kaposi's sarcoma-associated herpesvirus progeny requires formation of a pORF19 pentamer. *PLOS Biology* **19**:e3001423. DOI: https://doi.org/10.1371/journal.pbio.3001423

Newcomb WW, Brown JC. 1991. Structure of the herpes simplex virus capsid: effects of extraction with guanidine hydrochloride and partial reconstitution of extracted capsids. *Journal of Virology* **65**:613–620. DOI: https://doi.org/10.1128/jvi.65.2.613-620.1991, PMID: 1846187

Ojala PM, Sodeik B, Ebersold MW, Kutay U, Helenius A. 2000. Herpes Simplex Virus Type 1 Entry into Host Cells: Reconstitution of Capsid Binding and Uncoating at the Nuclear Pore Complex In Vitro. *Molecular and Cellular Biology* **20**:4922–4931. DOI: https://doi.org/10.1128/MCB.20.13.4922-4931.2000, PMID: 10848617

Page HG, Read GS. 2010. The Virion Host Shutoff Endonuclease (UL41) of Herpes Simplex Virus Interacts with the Cellular Cap-Binding Complex eIF4F. *Journal of Virology* **84**:6886–6890. DOI: https://doi.org/10.1128/JVI. 00166-10, PMID: 20427534

Paludan SR, Reinert LS, Hornung V. 2019. DNA-stimulated cell death: implications for host defence, inflammatory diseases and cancer. *Nature Reviews Immunology* **19**:141–153. DOI: https://doi.org/10.1038/ s41577-018-0117-0, PMID: 30644449

Pilla C, Emanuelli T, Frassetto SS, Battastini AM, Dias RD, Sarkis JJ. 1996. ATP diphosphohydrolase activity (apyrase, EC 3.6.1.5) in human blood platelets. *Platelets* **7**:225–230. DOI: https://doi.org/10.3109/ 09537109609023582, PMID: 21043691

Radtke K, Kieneke D, Wolfstein A, Michael K, Steffen W, Scholz T, Karger A, Sodeik B. 2010. Plus- and minus-end directed microtubule motors bind simultaneously to herpes simplex virus capsids using different inner tegument structures. *PLOS Pathogens* **6**:e1000991. DOI: https://doi.org/10.1371/journal.ppat.1000991, PMID: 20628567

Radtke K, Anderson F, Sodeik B. 2014. A precipitation-based assay to analyze interactions of viral particles with cytosolic host factors. *Methods in Molecular Biology* **1144**:191–208. DOI: https://doi.org/10.1007/978-1-4939- 0428-0_13, PMID: 24671685

Rode K, Döhner K, Binz A, Glass M, Strive T, Bauerfeind R, Sodeik B. 2011. Uncoupling uncoating of herpes simplex virus genomes from their nuclear import and gene expression. *Journal of Virology* **85**:4271–4283. DOI: https://doi.org/10.1128/JVI.02067-10, PMID: 21345968

Rodríguez MC, Dybas JM, Hughes J, Weitzman MD, Boutell C. 2020. The HSV-1 ubiquitin ligase ICP0: Modifying the cellular proteome to promote infection. *Virus Research* **285**:198015. DOI: https://doi.org/10.1016/j. virusres.2020.198015, PMID: 32416261

Roos WH, Radtke K, Kniesmeijer E, Geertsema H, Sodeik B, Wuite GJL. 2009. Scaffold expulsion and genome packaging trigger stabilization of herpes simplex virus capsids. *PNAS* **106**:9673–9678. DOI: https://doi.org/10. 1073/pnas.0901514106, PMID: 19487681

Rusinova I, Forster S, Yu S, Kannan A, Masse M, Cumming H, Chapman R, Hertzog PJ. 2013. Interferome v2.0: an updated database of annotated interferon-regulated genes. *Nucleic Acids Research* **41**:D1040–D1046. DOI: https://doi.org/10.1093/nar/gks1215, PMID: 23203888

Sae-Ueng U, Liu T, Catalano CE, Huffman JB, Homa FL, Evilevitch A. 2014. Major capsid reinforcement by a minor protein in herpesviruses and phage. *Nucleic Acids Research* **42**:9096–9107. DOI: https://doi.org/10. 1093/nar/gku634, PMID: 25053840

Sandbaumhüter M, Döhner K, Schipke J, Binz A, Pohlmann A, Sodeik B, Bauerfeind R. 2013. Cytosolic herpes simplex virus capsids not only require binding inner tegument protein pUL36 but also pUL37 for active transport prior to secondary envelopment. *Cellular Microbiology* **15**:248–269. DOI: https://doi.org/10.1111/ cmi.12075, PMID: 23186167

Schilling M, Bulli L, Weigang S, Graf L, Naumann S, Patzina C, Wagner V, Bauersfeld L, Goujon C, Hengel H, Halenius A, Ruzsics Z, Schaller T, Kochs G. 2018. Human MxB Protein Is a Pan-herpesvirus Restriction Factor. *Journal of Virology* **92**:e01056-18. DOI: https://doi.org/10.1128/JVI.01056-18, PMID: 29950411

Schipke J, Pohlmann A, Diestel R, Binz A, Rudolph K, Nagel CH, Bauerfeind R, Sodeik B. 2012. The C terminus of the large tegument protein pUL36 contains multiple capsid binding sites that function differently during assembly and cell entry of herpes simplex virus. *Journal of Virology* **86**:3682–3700. DOI: https://doi.org/10. 1128/JVI.06432-11, PMID: 22258258

Schneider SM, Lee BH, Nicola AV. 2021. Viral entry and the ubiquitin-proteasome system. *Cellular Microbiology* **23**:e13276. DOI: https://doi.org/10.1111/cmi.13276, PMID: 33037857

Schulte B, Buffone C, Opp S, Di Nunzio F, De Souza Aranha Vieira DA, Brandariz-Nuñez A, Diaz-Griffero F. 2015. Restriction of HIV-1 Requires the N-Terminal Region of MxB as a Capsid-Binding Motif but Not as a Nuclear Localization Signal. *Journal of Virology* **89**:8599–8610. DOI: https://doi.org/10.1128/JVI.00753-15, PMID: 26063425

Shannon P, Markiel A, Ozier O, Baliga NS, Wang JT, Ramage D, Amin N, Schwikowski B, Ideker T. 2003. Cytoscape: a software environment for integrated models of biomolecular interaction networks. *Genome Research* **13**:2498–2504. DOI: https://doi.org/10.1101/gr.1239303, PMID: 14597658

Smaga SS, Xu C, Summers BJ, Digianantonio KM, Perilla JR, Xiong Y. 2019. MxB Restricts HIV-1 by Targeting the Tri-hexamer Interface of the Viral Capsid. *Structure* **27**:1234–1245. DOI: https://doi.org/10.1016/j.str.2019.04. 015, PMID: 31155311

Snijder J, Radtke K, Anderson F, Scholtes L, Corradini E, Baines J, Heck AJR, Wuite GJL, Sodeik B, Roos WH. 2017. Vertex-Specific Proteins pUL17 and pUL25 Mechanically Reinforce Herpes Simplex Virus Capsids. *Journal of Virology* **91**:e00123-17. DOI: https://doi.org/10.1128/JVI.00123-17, PMID: 28381566

Stempel M, Chan B, Brinkmann MM. 2019. Coevolution pays off: Herpesviruses have the license to escape the DNA sensing pathway. *Medical Microbiology and Immunology* **208**:495–512. DOI: https://doi.org/10.1007/ s00430-019-00582-0, PMID: 30805724

Sumner RP, Harrison L, Touizer E, Peacock TP, Spencer M, Zuliani-Alvarez L, Towers GJ. 2020. Disrupting HIV-1 capsid formation causes cGAS sensing of viral DNA. *The EMBO Journal* **39**:e103958. DOI: https://doi.org/10. 15252/embj.2019103958, PMID: 32852081

Sun C, Luecke S, Bodda C, Jønsson KL, Cai Y, Zhang B-C, Jensen SB, Nordentoft I, Jensen JM, Jakobsen MR, Paludan SR. 2019. Cellular Requirements for Sensing and Elimination of Incoming HSV-1 DNA and Capsids. *Journal of Interferon & Cytokine Research* **39**:191–204. DOI: https://doi.org/10.1089/jir.2018.0141, PMID: 30855198

Szklarczyk D, Gable AL, Lyon D, Junge A, Wyder S, Huerta-Cepas J, Simonovic M, Doncheva NT, Morris JH, Bork P, Jensen LJ, Mering C. 2019. STRING v11: protein-protein association networks with increased coverage, supporting functional discovery in genome-wide experimental datasets. *Nucleic Acids Research* **47**:D607–D613. DOI: https://doi.org/10.1093/nar/gky1131, PMID: 30476243

Temple J, Tripler TN, Shen Q, Xiong Y. 2020. A snapshot of HIV-1 capsid–host interactions. *Current Research in Structural Biology* **2**:222–228. DOI: https://doi.org/10.1016/j.crstbi.2020.10.002, PMID: 34113849

Tsuchiya S, Yamabe M, Yamaguchi Y, Kobayashi Y, Konno T, Tada K. 1980. Establishment and characterization of a human acute monocytic leukemia cell line (THP-1). *International Journal of Cancer* **26**:171–176. DOI: https://doi.org/10.1002/ijc.2910260208, PMID: 6970727

Turan A, Grosche L, Krawczyk A, Mühl-Zürbes P, Drassner C, Düthorn A, Kummer M, Hasenberg M, Voortmann S, Jastrow H, Dörrie J, Schaft N, Kraner M, Döhner K, Sodeik B, Steinkasserer A, Heilingloh CS. 2019. Autophagic degradation of lamins facilitates the nuclear egress of herpes simplex virus type 1. *The Journal of Cell Biology* **218**:508–523. DOI: https://doi.org/10.1083/jcb.201801151, PMID: 30587512

Tyanova S, Temu T, Cox J. 2016a. The MaxQuant computational platform for mass spectrometry-based shotgun proteomics. *Nature Protocols* **11**:2301–2319. DOI: https://doi.org/10.1038/nprot.2016.136, PMID: 27809316

Tyanova S, Temu T, Sinitcyn P, Carlson A, Hein MY, Geiger T, Mann M, Cox J. 2016b. The Perseus computational platform for comprehensive analysis of (prote)omics data. *Nature Methods* **13**:731–740. DOI: https://doi.org/10.1038/nmeth.3901, PMID: 27348712

Warner MS, Geraghty RJ, Martinez WM, Montgomery RI, Whitbeck JC, Xu R, Eisenberg RJ, Cohen GH, Spear PG. 1998. A cell surface protein with herpesvirus entry activity (HveB) confers susceptibility to infection by mutants of herpes simplex virus type 1, herpes simplex virus type 2, and pseudorabies virus. *Virology* **246**:179–189. DOI: https://doi.org/10.1006/viro.1998.9218, PMID: 9657005

Whitley R, Roizman B. 2016. Herpes Simplex Viruses. Richman DD, Whitley RJ, Hayden FJ (Eds). *Clinical Virology, Fourth Edition*. ASM Press. p. 415–445. DOI: https://doi.org/10.1128/9781555819439

Whitley R, Johnston C. 2021. Herpes Simplex Viruses: Pathogenesis and Clinical Insights. Howley PM, Knipe DM, Cohen JL, Damania BA (Eds). *In Fields Virology: DNA Viruses*. Wolters Kluwer Health/Lippincott Williams & Wilkins. p. 297–323.

Wolfstein A, Nagel CH, Radtke K, Döhner K, Allan VJ, Sodeik B. 2006. The inner tegument promotes herpes simplex virus capsid motility along microtubules in vitro. *Traffic* **7**:227–237. DOI: https://doi.org/10.1111/j.1600-0854.2005.00379.x, PMID: 16420530

Xie L, Ju Z, Zhong C, Wu Y, Zan Y, Hou W, Feng Y. 2021. GTPase Activity of MxB Contributes to Its Nuclear Location, Interaction with Nucleoporins and Anti-HIV-1 Activity. *Virologica Sinica* **36**:85–94. DOI: https://doi.org/10.1007/s12250-020-00249-8, PMID: 32632818

Zenner HL, Yoshimura S-I, Barr FA, Crump CM. 2011. Analysis of Rab GTPase-activating proteins indicates that Rab1a/b and Rab43 are important for herpes simplex virus 1 secondary envelopment. *Journal of Virology* **85**:8012–8021. DOI: https://doi.org/10.1128/JVI.00500-11, PMID: 21680502

Zhang Y, McKnight JL. 1993. Herpes simplex virus type 1 UL46 and UL47 deletion mutants lack VP11 and VP12 or VP13 and VP14, respectively, and exhibit altered viral thymidine kinase expression. *Journal of Virology* **67**:1482–1492. DOI: https://doi.org/10.1128/JVI.67.3.1482-1492.1993, PMID: 8382306

Zhang Z, Kim T, Bao M, Facchinetti V, Jung SY, Ghaffari AA, Qin J, Cheng G, Liu YJ. 2011. DDX1, DDX21, and DHX36 helicases form a complex with the adaptor molecule TRIF to sense dsRNA in dendritic cells. *Immunity* **34**:866–878. DOI: https://doi.org/10.1016/j.immuni.2011.03.027, PMID: 21703541